CHAPTER 8

SUGGESTION FOR FURTHER WORK

(1) From the expressions that at R = 5r for unreinforced and R = 7r for reinforced ninety degree mitered pipe bends, these bends will have same flexibility as that of smooth bends of same dimensions, these results are abtained on hot rolled steel. For future work, various materials such as other kinds of iron, steel or brass should be tested and compare the results with these obtained here to find whether these expressions can be used for all kinds of material.

(2) In this experimental work for stresses, it is analysed only stresses at the same circular section on pipe surface for the reinforced ninety degree mitered pipe bend. Unreinforced ninety degree mitered pipe bend should be analysed also and compare the results with those of the reinforced bend.

(3) The variation of stresses along the whole pipe length at outer and inner surfaces of ninety degree single mitered pipe bend with reinforced and unreinforced should be determined next.

(4) Also the variation of stresses due to in-plane bending moment around the circular section of the pipe at the inner surface should be investigated and compared with the

values at the outer surface.

(5) On the theoretical side, the more applicable theoretical analysis for the bending stresses around the pipe should be attempted using the evidence from the experimental results obtained here.

APPENDIX I

STRAIN GAGE TECHNIQUE

The principle of the electric resistance strain gage was discovered by Lord Kelvin when he observed that the resistance of a wire alters when it is subjected to stress.

A typical strain gage element consists of a continuous length of resistance wire of about 0.001 in diameter wound as indicated in Fig. I and cemented to a paper backing.

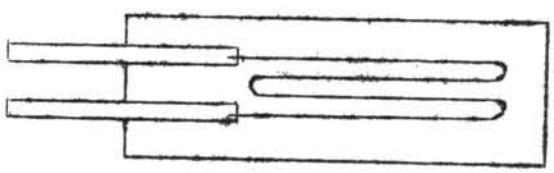

Fig. I WIRE-WOUND STRAIN GAGE ELEMENT

The strain gage is cemented to the material in which it is required to measure the strain. As the test specimen extends or contracts under stress in the direction of the windings, the length and cross-sectional area of the resistance wire alter, resulting in a corresponding increase or decrease in electrical resistance. The essential property of the resistive element is that resistance varies with strain. This property is defined in terms of the gage factor f. By definition :

$$f = \frac{\Delta R/R}{\Delta L/L} = \frac{\Delta R/R}{e}$$

in which

f = gage factor

R = electrical resistance

L = length of strain-sensitive element

e = normal or axial strain

Therefore, to find the strain, e we only have to find ΔR as f and R is given.

On the basis of the change of length and cross-sectional area only, it can be shown that the gage factor would be

$$f = (1 + 2\mu) + \frac{d\rho}{\rho}_{e}$$ (from Ref.(6) pp. 50-53)

where μ = Poisson's ratio.

ρ = specfic resistance of the material

Continuous relaxation of the material insures that the specific resistivity remain constant (i.e. $\frac{d\rho/\rho}{e} = 0$) then $f = 1 + 2\mu$

The most important procedure in resistant strain gage work is the mounting of the gage element on the surface of the test piece. The surface must first be smoothed by grade O emery cloth and thoroughly degreased by carbontetrachloride or acetone. In general, a thin layer of cement is first applied to the surface and allowed to dry out. A second layer of cement is then applied and the gage pressed into position with a rolling movement so that the surplus adhesive is expelled at the ends of the gage. It is essential to

protect the gage from moisture if measurements are to be taken over a prolonged period. Absorption of moisture by the gage matrix may result in an apparent reduction of the gage factor and in extreme cases passage of current through a damp gage can result in failure of the wire due to corrosion. Ingress of moisture can be prevented by coating the gage with Vaseline or Di Jell 171. After mounting and wiring up, each strain gage element should be checked for resistance before connecting to sensitive equipment.

In this experiment KYOWA Japanese strain gage and strain gage cement, type BC-11 as shown in Fig. A39 were used. Acetone was used to degrease the surface and prevent the ingress of moisture by coating the gage with Vaseline. These strain gage were then wired to external apex units and selector switch and to the strain gage bridge as shown in schematic diagrams Fig. A-24. and A-25. These figures demonstrate the connection of the strain gages to the bridge. The state of the battery was frequently checked and recharge was carried out when the pointer of the meter failed to reach the red line. The gage factor dial of the bridge was set to the value of the gage factor of strain gage, which is at 2.1. Switch SW. 1 as shown in Fig. A23. was turned to "on" position. The gages were balanced for zero with the same kind of gage free from strain. The measuring dial was set to zero. The detector button was pressed and the apex was adjusted to bring the gavanometer pointer to the zero position. If the bridge

could not be balanced, the resistance of the two strain gages should be checked. The maximum difference of resistance of the gages should not be more than 0.04 ohms at the initial balancing. When loaded, the measuring dial was turned to bring the pointer of the galvanometer to zero position then percent elongation or percent strain could be read. If "pull for $\frac{1}{10}$" button was pulled, percent strain obtained would be the percent strain reading devided by 10. For the bridge used, the percent strain in the ranges of -0.1 to 0.1 % and -1 to 1 % could be measured.

In this research the value of both axial and circumferential strains have not been corrected. Although there is some effect from cross-strain sensitivities but the author thought that this effect is small compared to other effects such as the length of strain gages.

APPENDIX II

From the assumption that shear strain varied from zero at ±90 degree positions to maximum value at 0 degree position in the form of parabolic curve

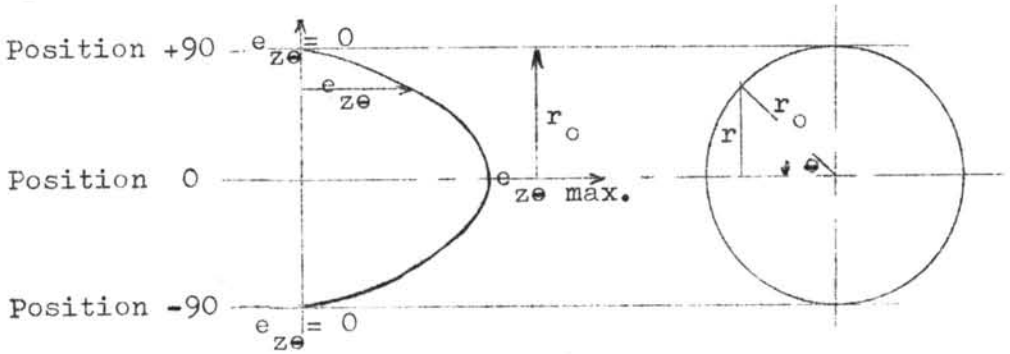

Fig. II VARITION OF SHEAR STRAIN ON z-θ PLANE.

$$r^2 = C(e_{z\theta_{max}} - e_{z\theta}) \qquad (1)$$

boundary condition : $e_{z\theta} = 0$ at $r = r_o$

hence $r_o^2 = Ce_{z\theta\ max}$

substitute in (1) and re-arrange

$$e_{z\theta} = e_{z\theta\ max}\left(1 - \frac{r^2}{r_o^2}\right)$$

but $r = r_o \sin\theta$

then $e_{z\theta} = e_{z\theta\ max}(1 - \sin^2\theta)$

$= e_{z\theta\ max}.\cos^2\theta$

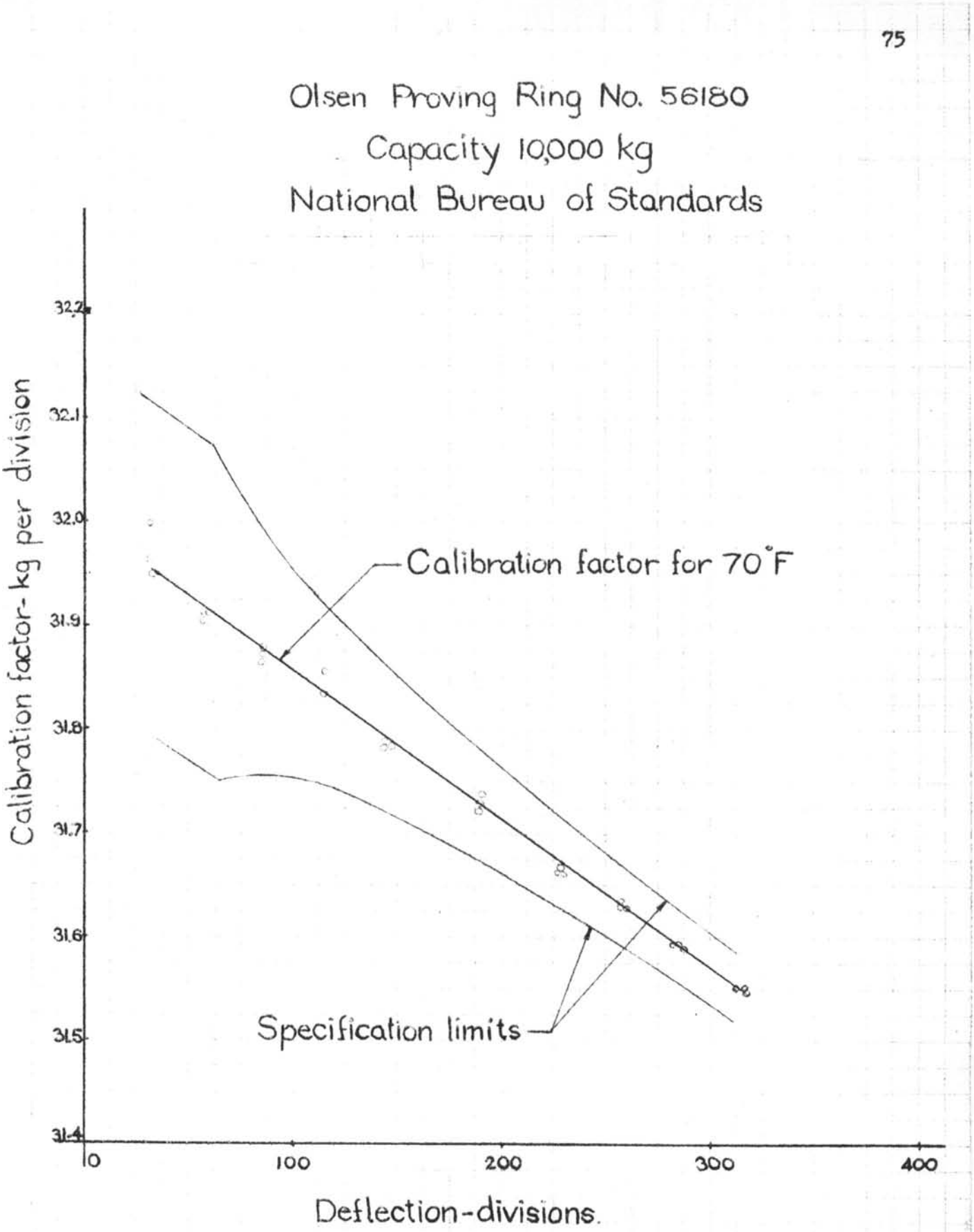

Fig. A1. CALIBRATION CURVE OF PROVING RING NO. 56180.

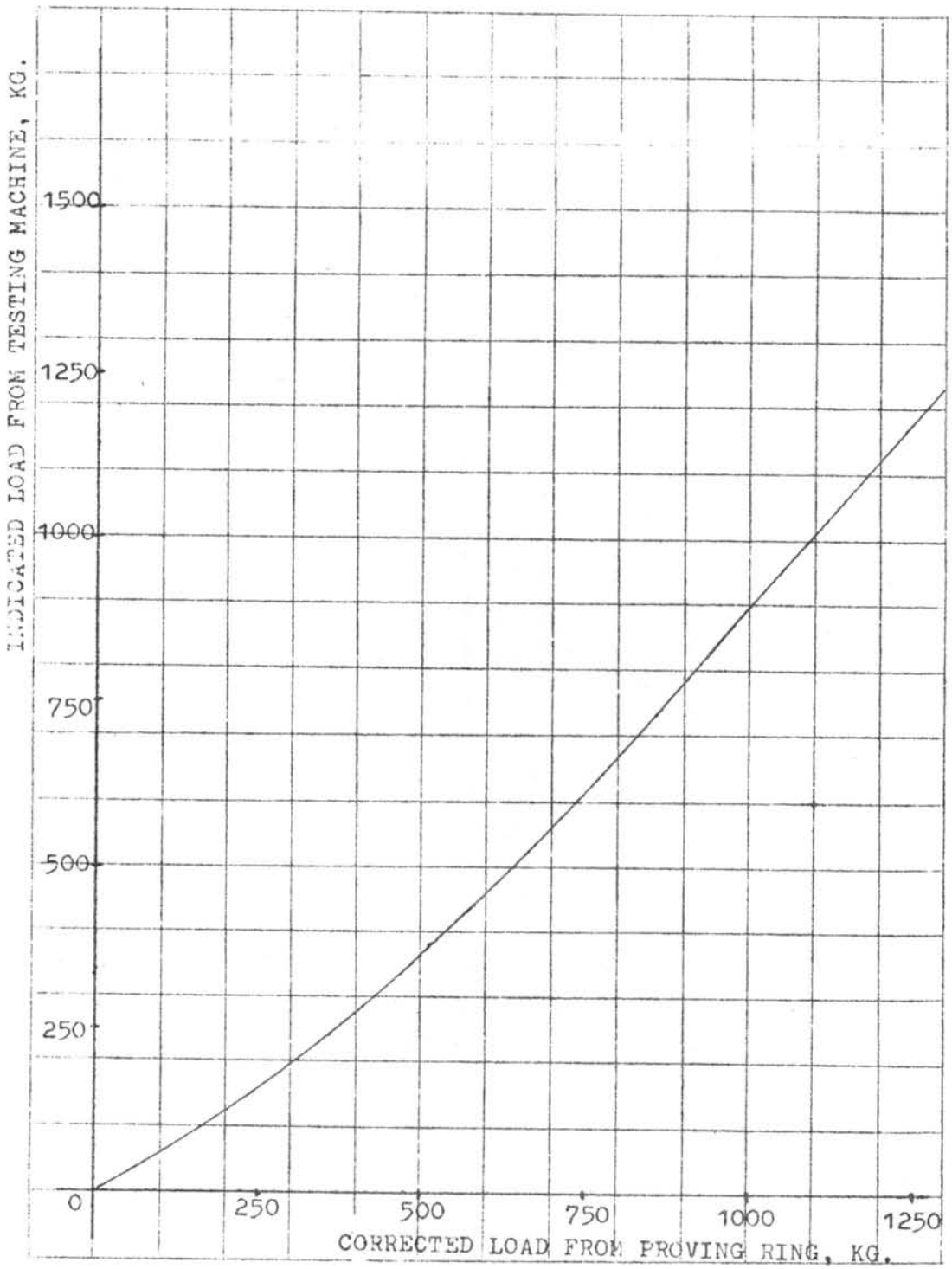

Fig. A2. CALIBRATION CURVE OF "AVERY" TESTING MACHINE NO. E. 66110 CAPACITY 15000 KG (6000 KG) LOAD RANGE 0-3000 LB (0-1360 KG)

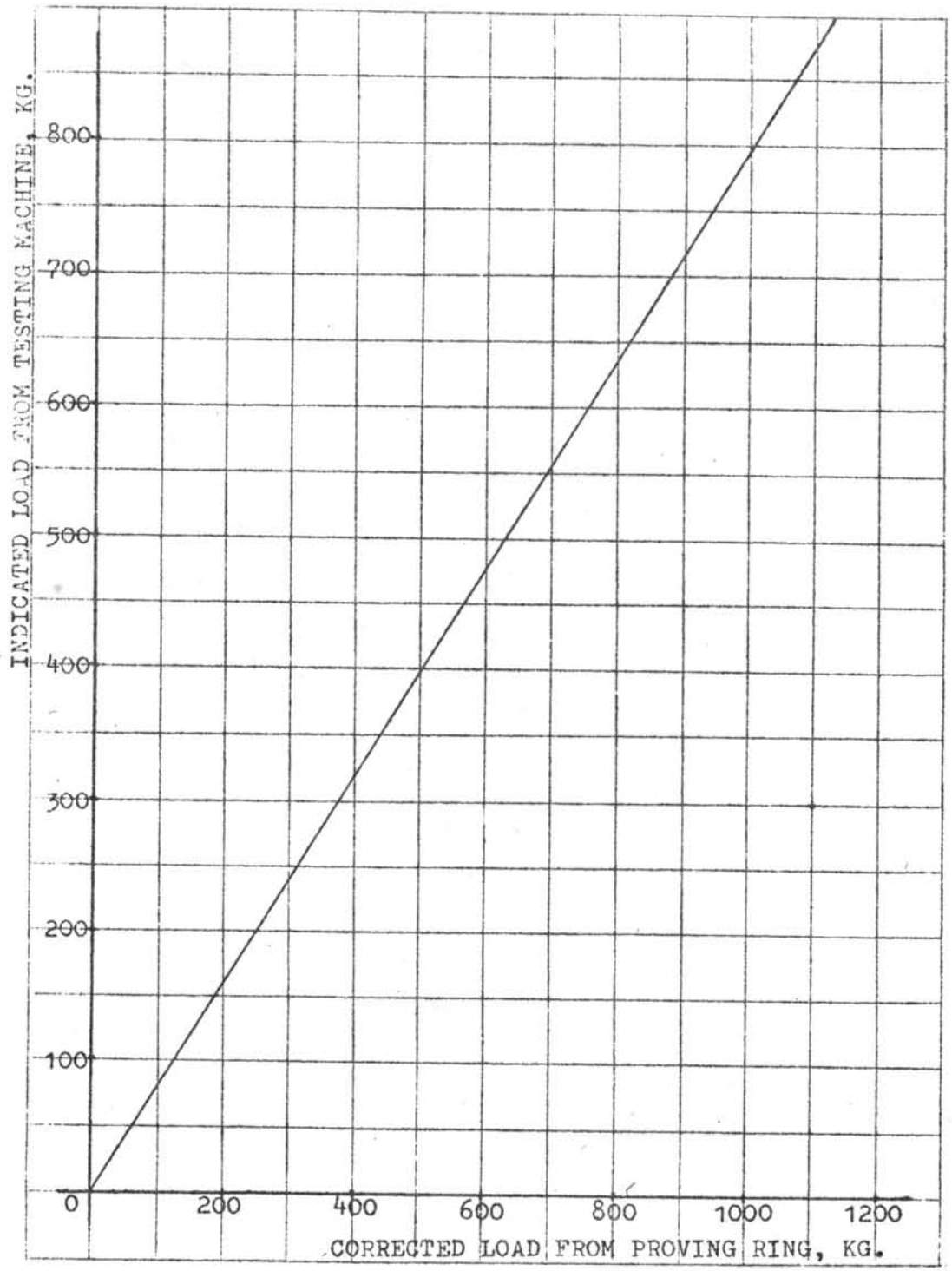

Fig. A3. CALIBRATION CURVE OF "AMSLER" TESTING MACHINE NO. 060355AK CAPACITY 20 TONS, LOAD RANGE 0-2 TONS.

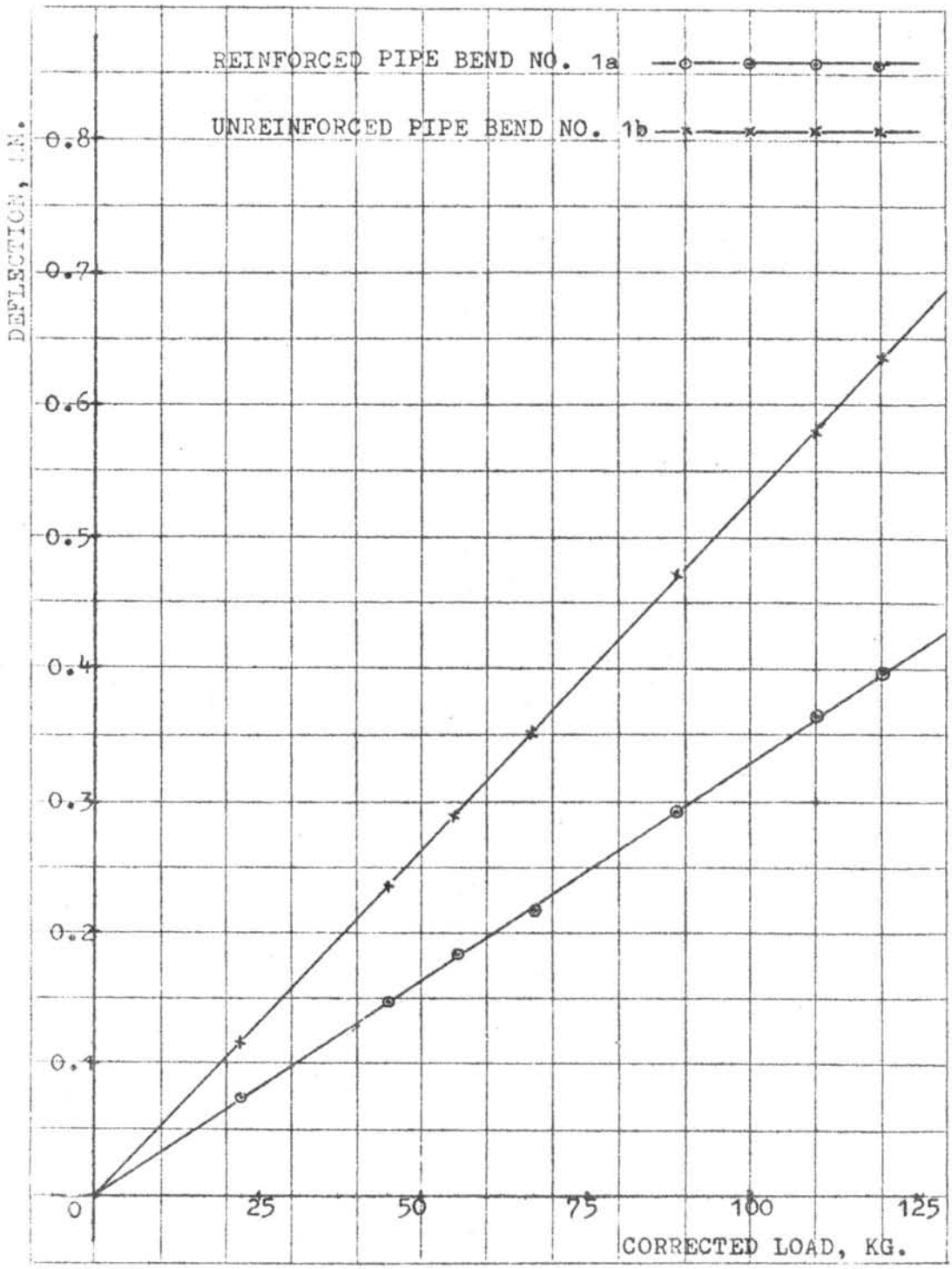

Fig. A4. DEFLECTION UNDER IN-PLANE BENDING.

(PIPE BENDS NO. 1a, 1b)

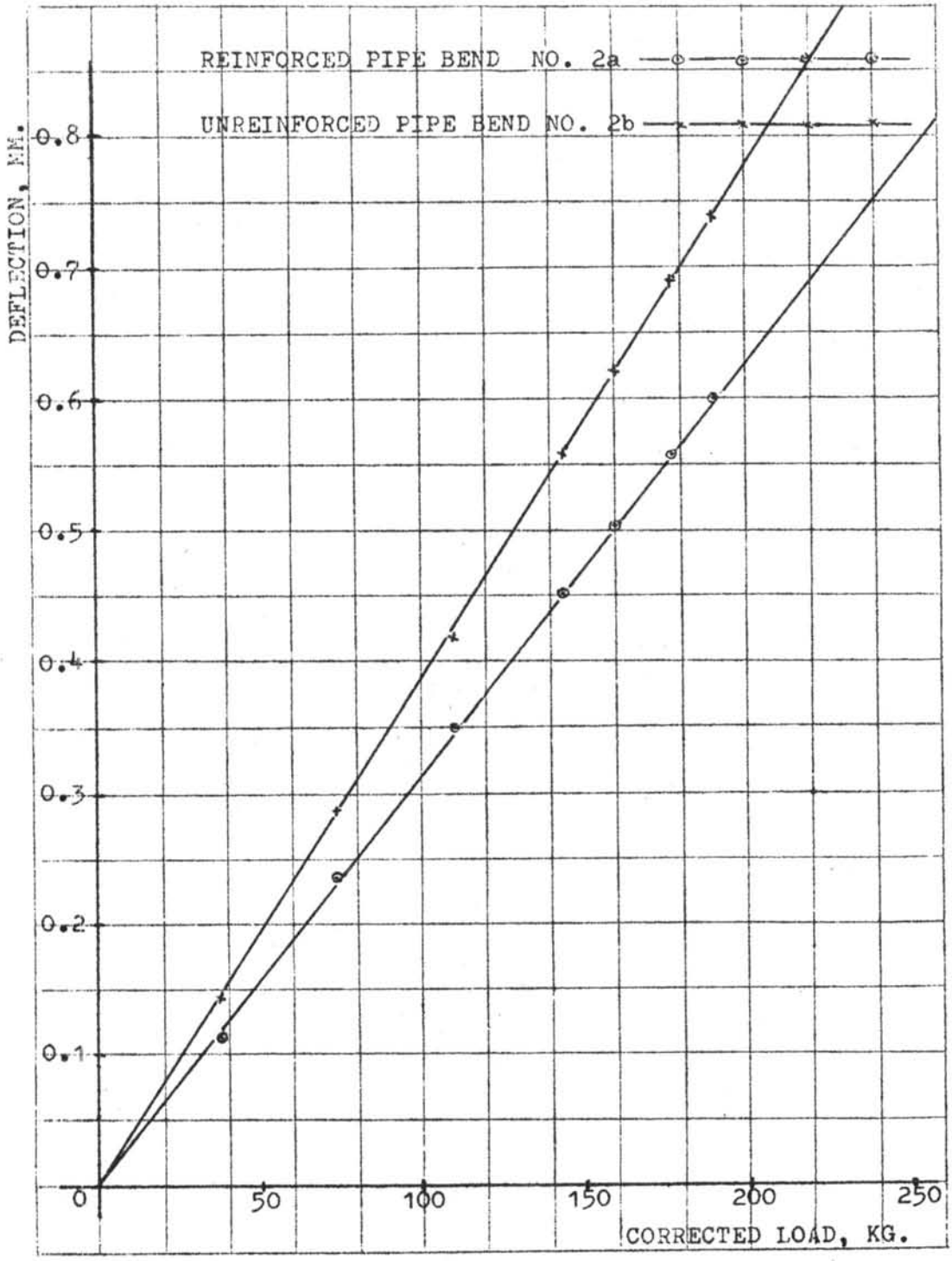

Fig. A5. DEFLECTION UNDER IN-PLANE BENDING.

(PIPE BENDS NO. 2a,2b)

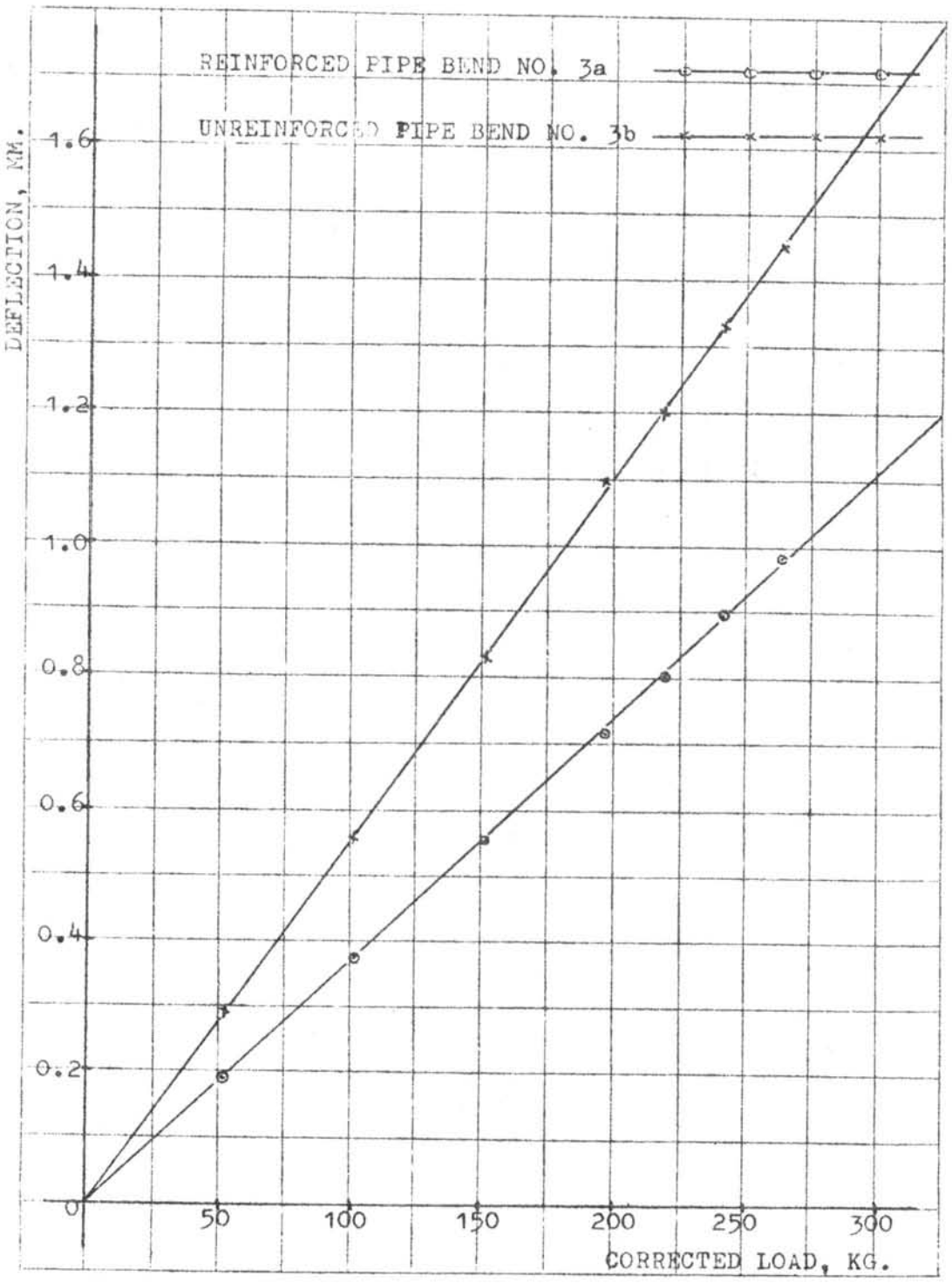

Fig. A6. DEFLECTION UNDER IN-PLANE BENDING.

(PIPE BENDS NO. 3a, 3b)

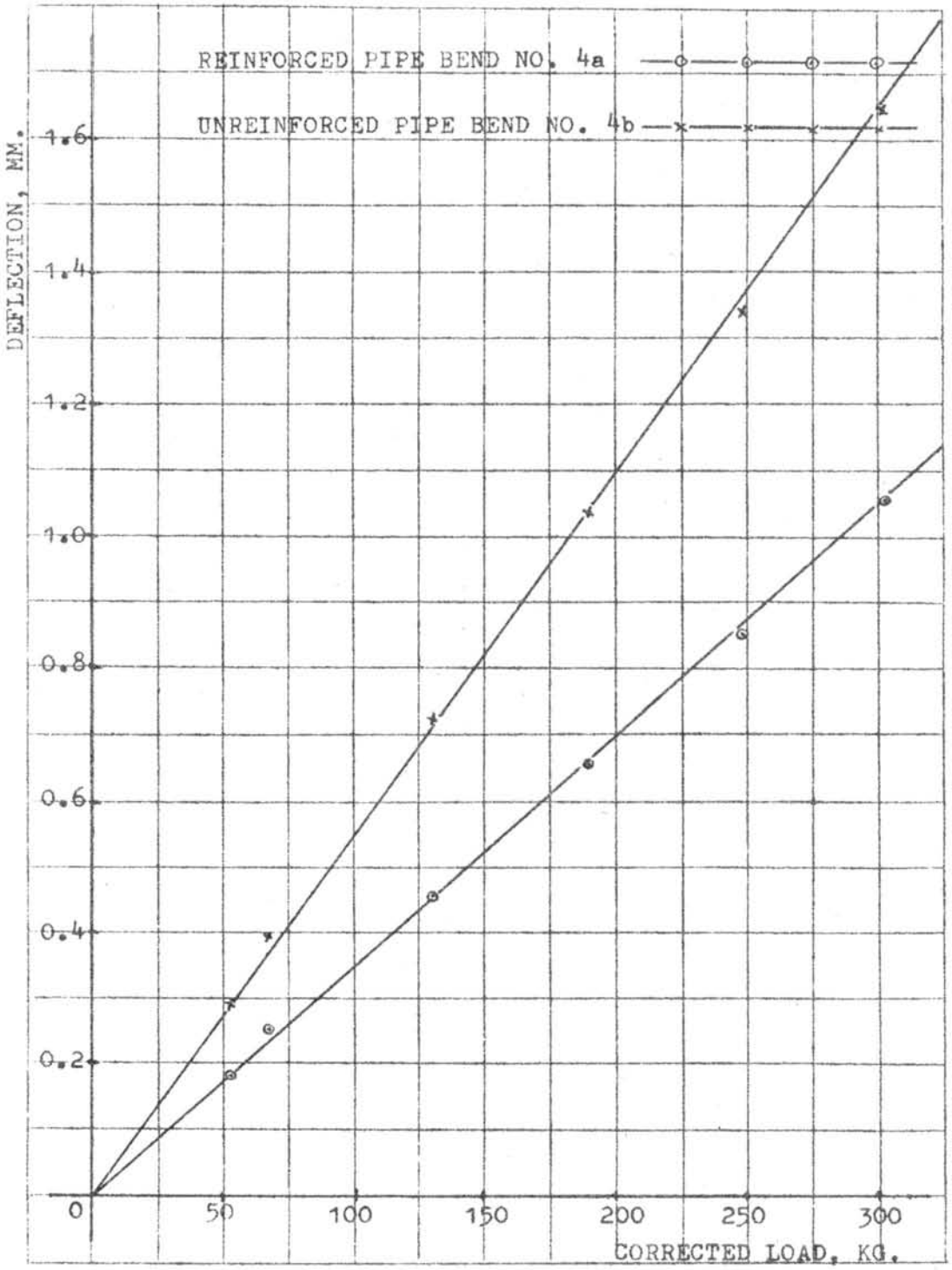

Fig. A7 DEFLECTION UNDER IN-PLANE BENDING.

(PIPE BENDS NO. 4a,4b)

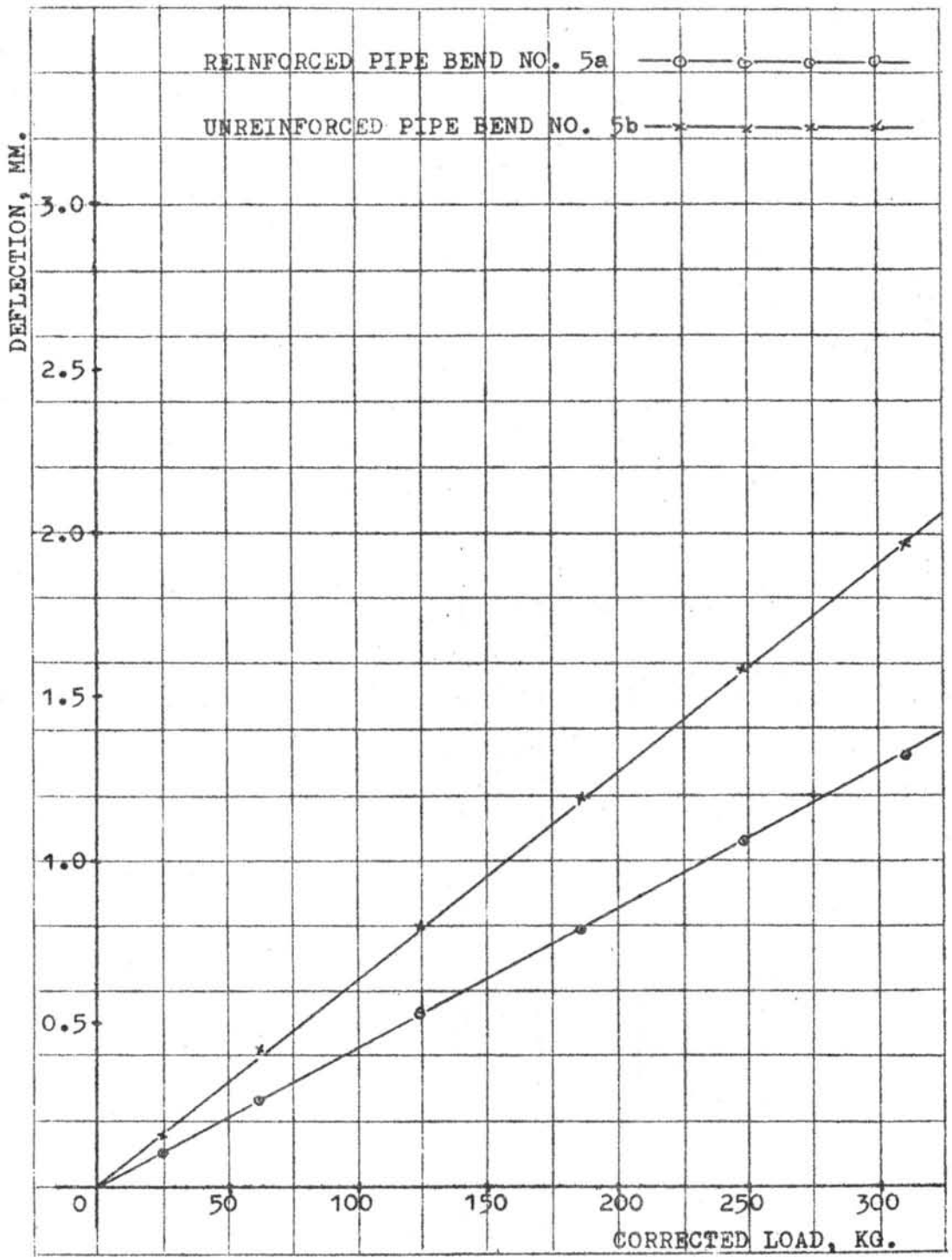

Fig. A8. DEFLECTION UNDER IN-PLANE BENDING.

(PIPE BENDS NO. 5a,5b)

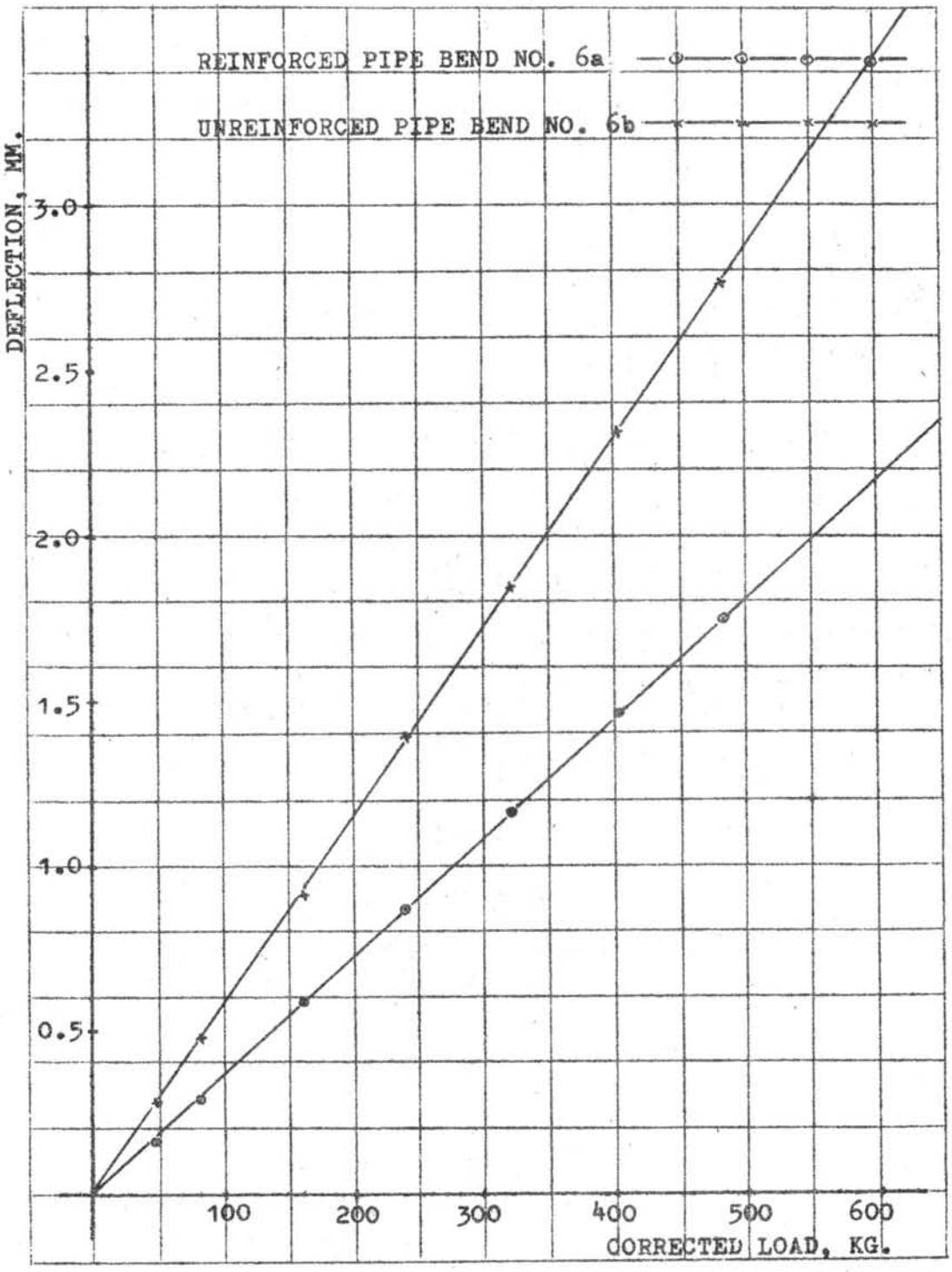

Fig. A9. DEFLECTION UNDER IN-PLANE BENDING.

(PIPE BENDS NO. 6a, 6b)

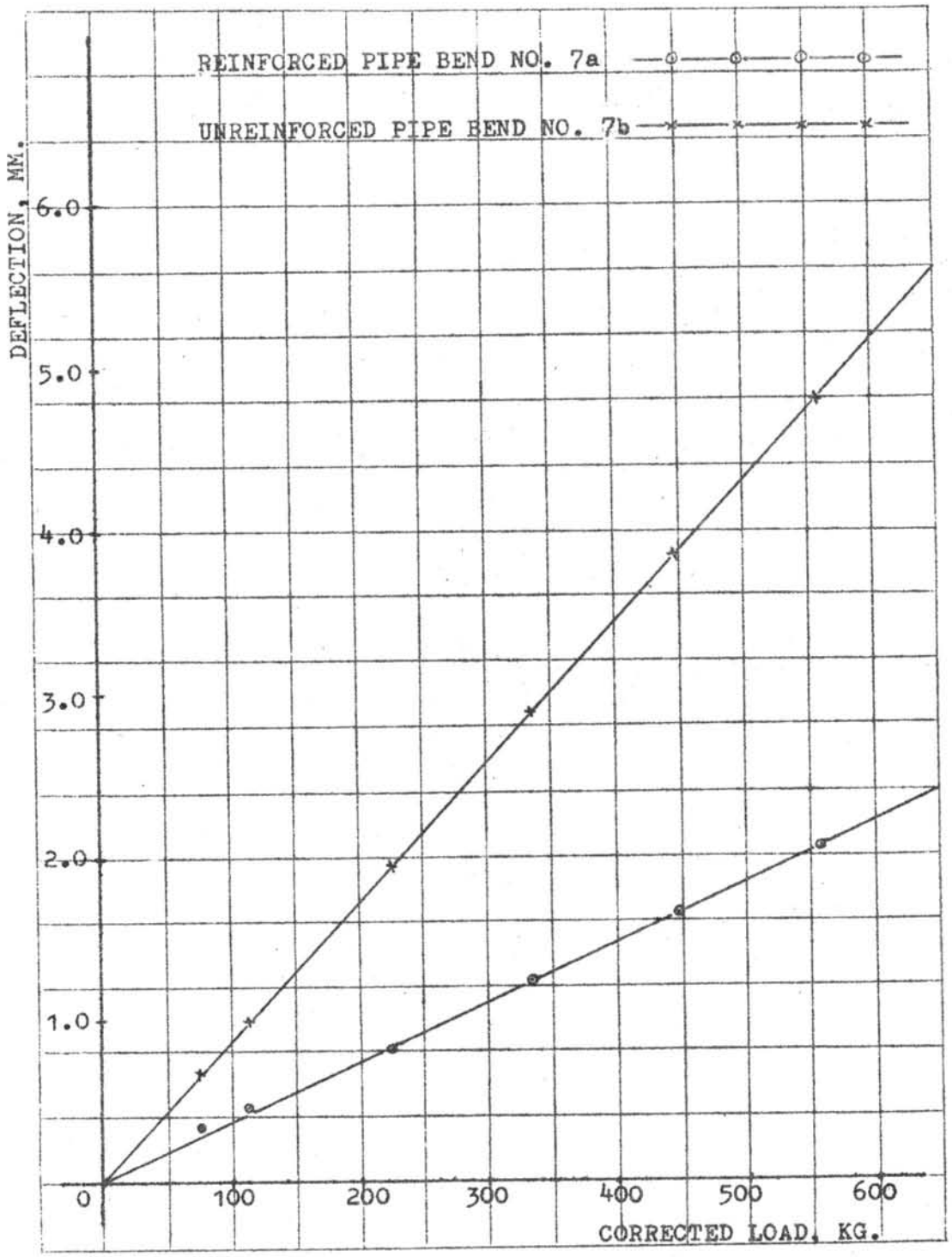

Fig. A10. DEFLECTION UNDER IN-PLANE BENDING.

(PIPE BENDS NO. 7a,7b)

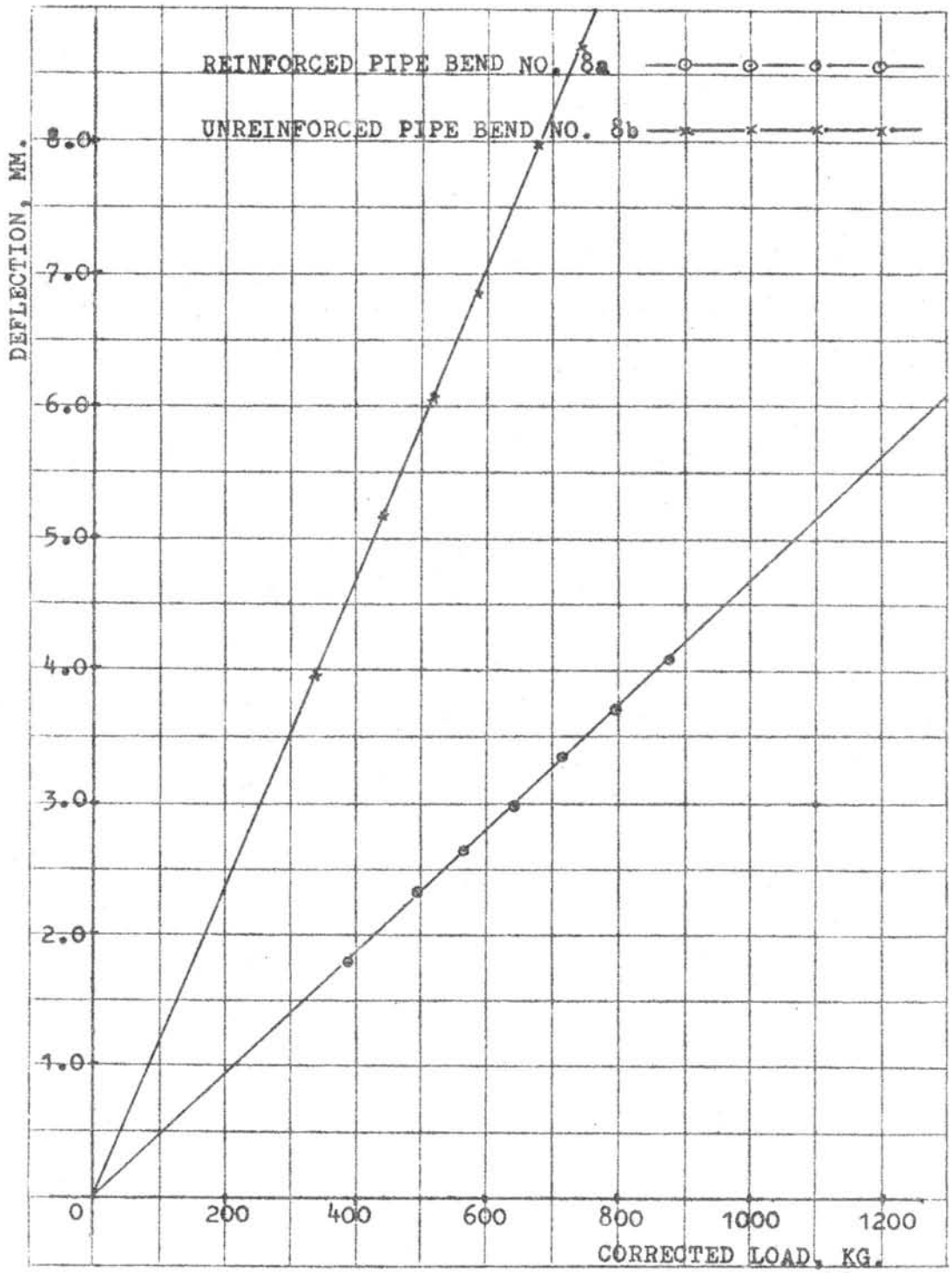

Fig. A11. DEFLECTION UNDER IN-PLANE BENDING.

(PIPE BENDS NO. 8a,8b)

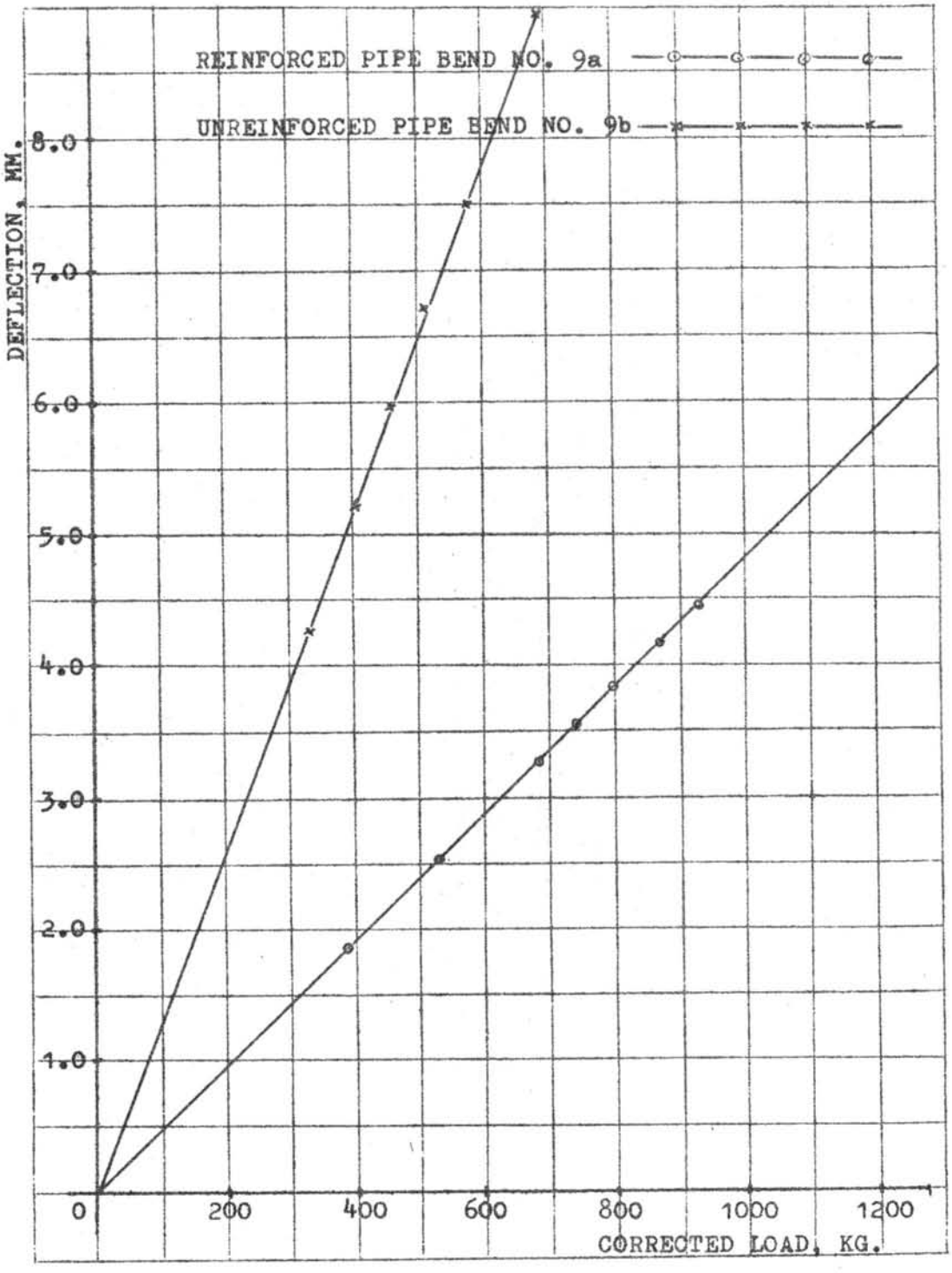

Fig. A12. DEFLECTION UNDER IN-PLANE BENDING.

(PIPE BENDS NO. 9a,9b)

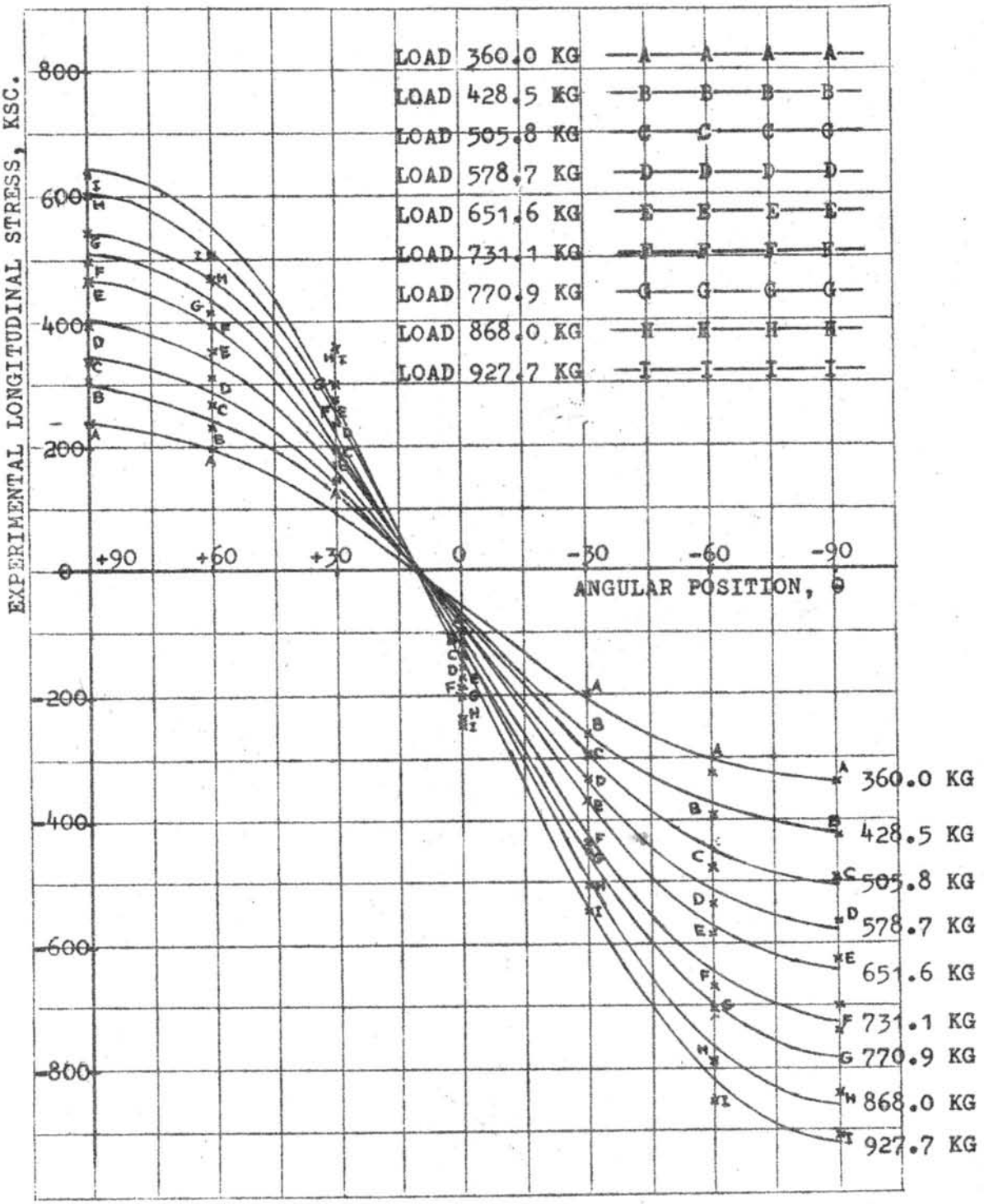

Fig. A13. VARIATION OF EXPERIMENTAL LONGITUDINAL STRESS AROUND PIPE.

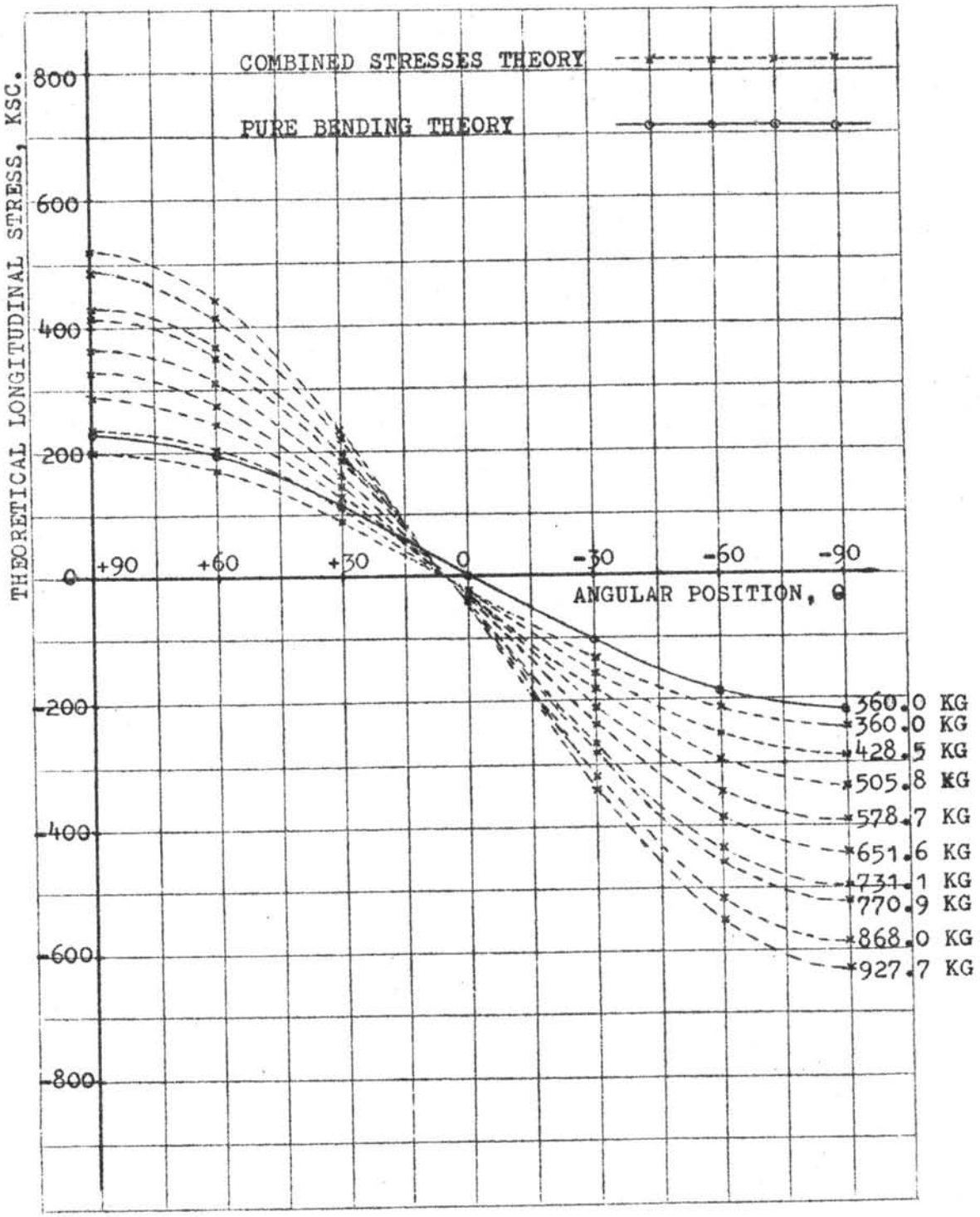

Fig. A14. VARIATION OF THEORETICAL LONGITUDINAL STRESS AROUND PIPE.

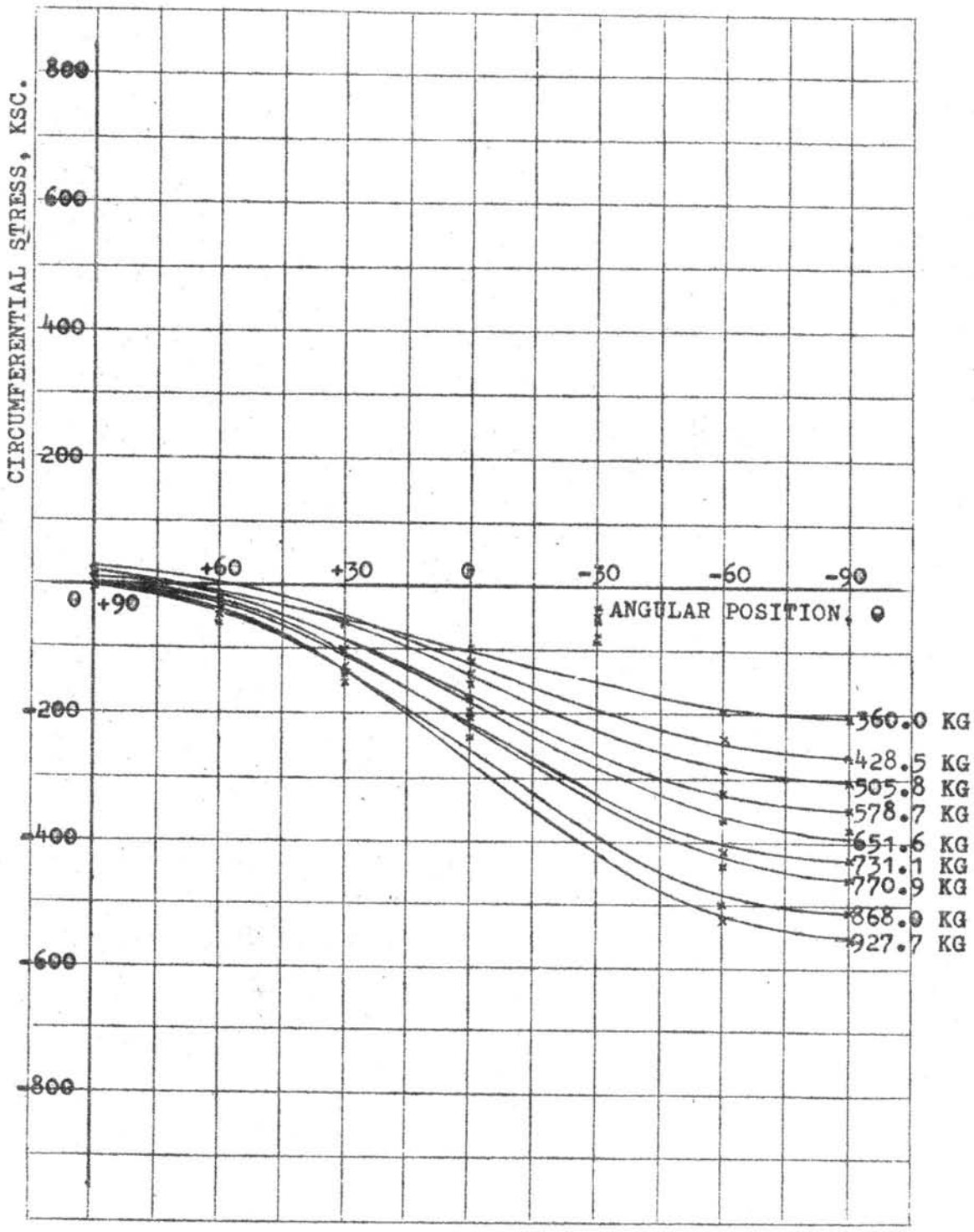

Fig. A15. VARIATION OF CIRCUMFERENTIAL STRESS AROUND PIPE.

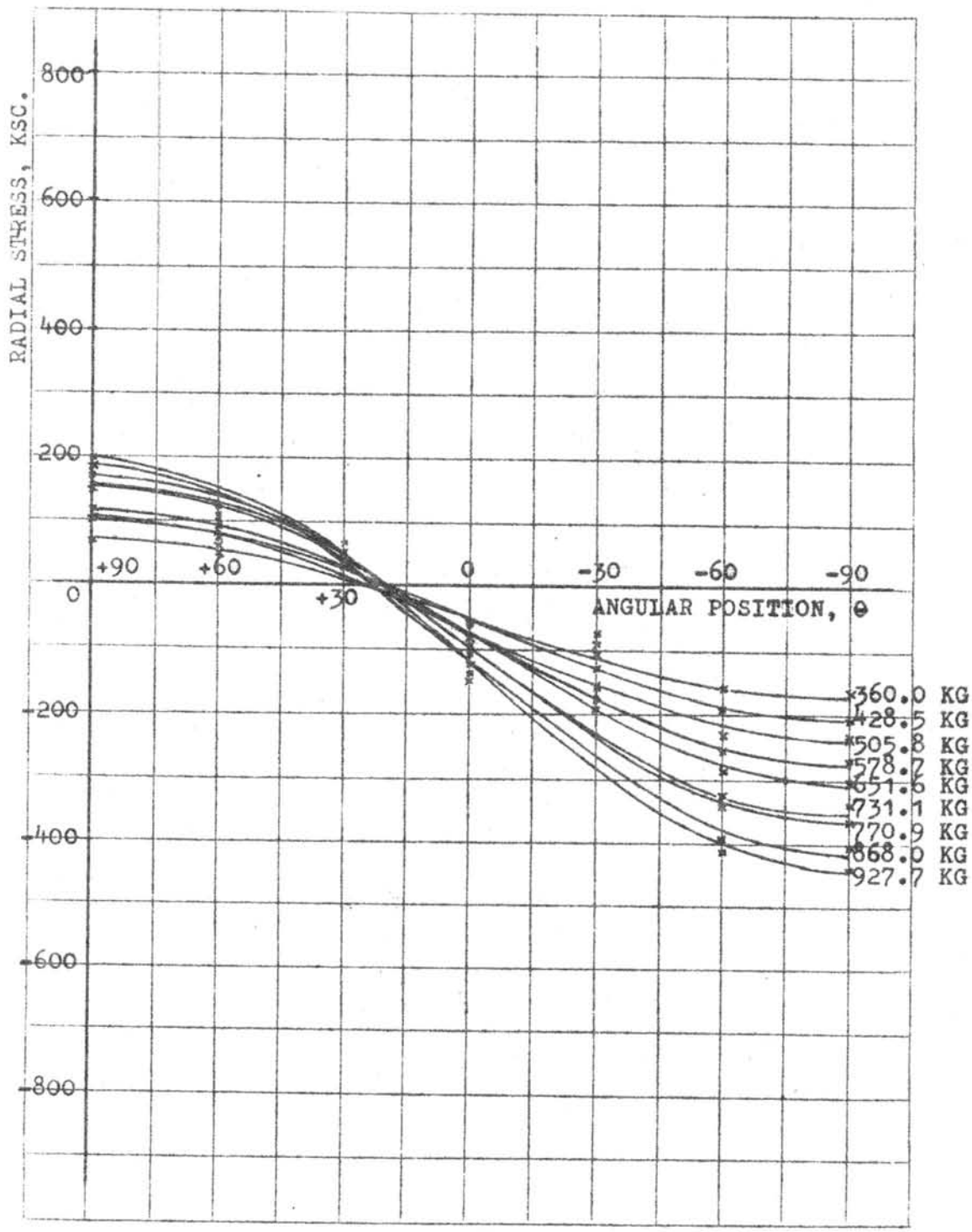

Fig. A16. VARIATION OF RADIAL STRESS AROUND PIPE.

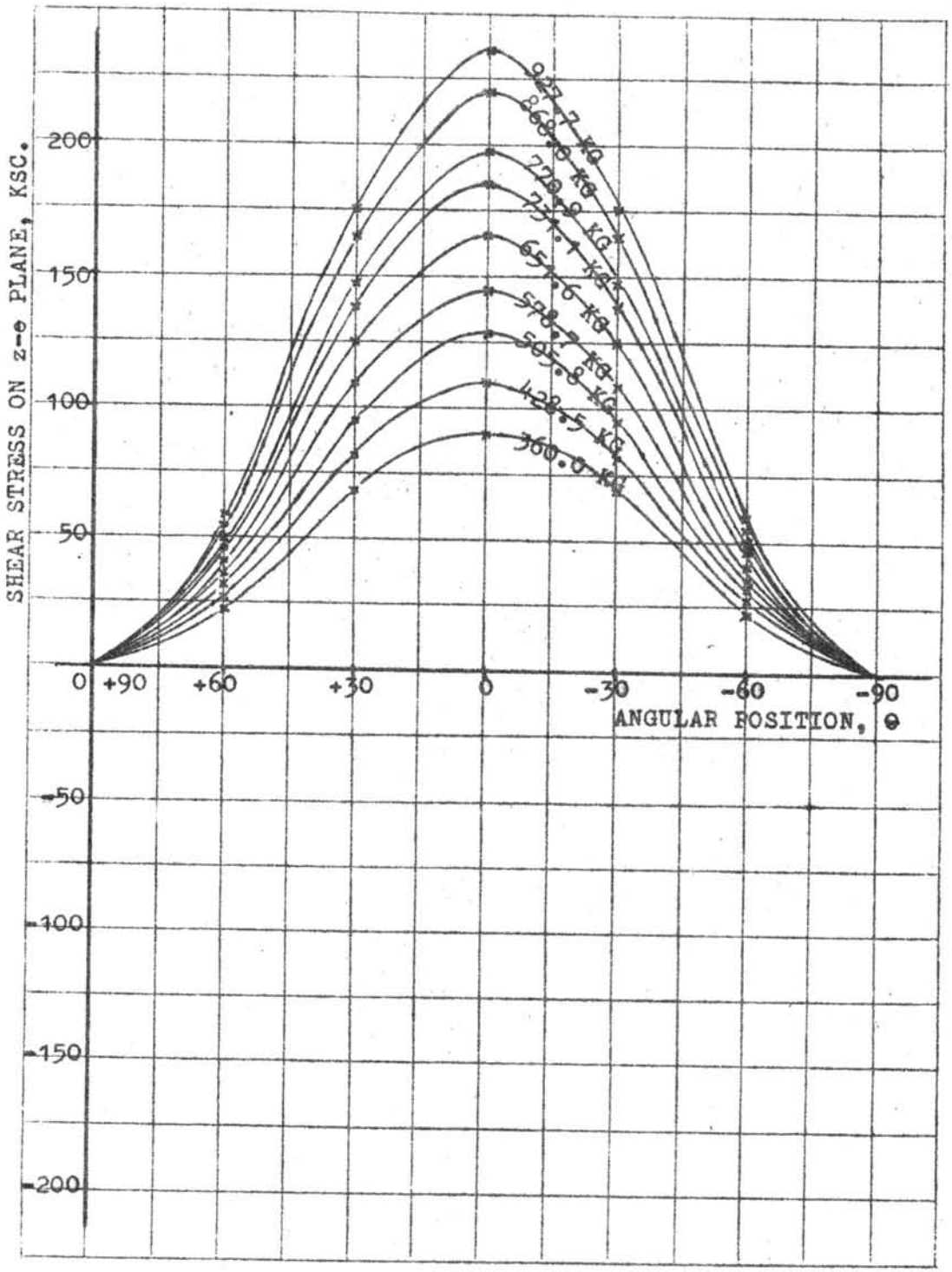

Fig. A17. VARIATION OF SHEAR STRESS ON z-θ PLANE AROUND PIPE.

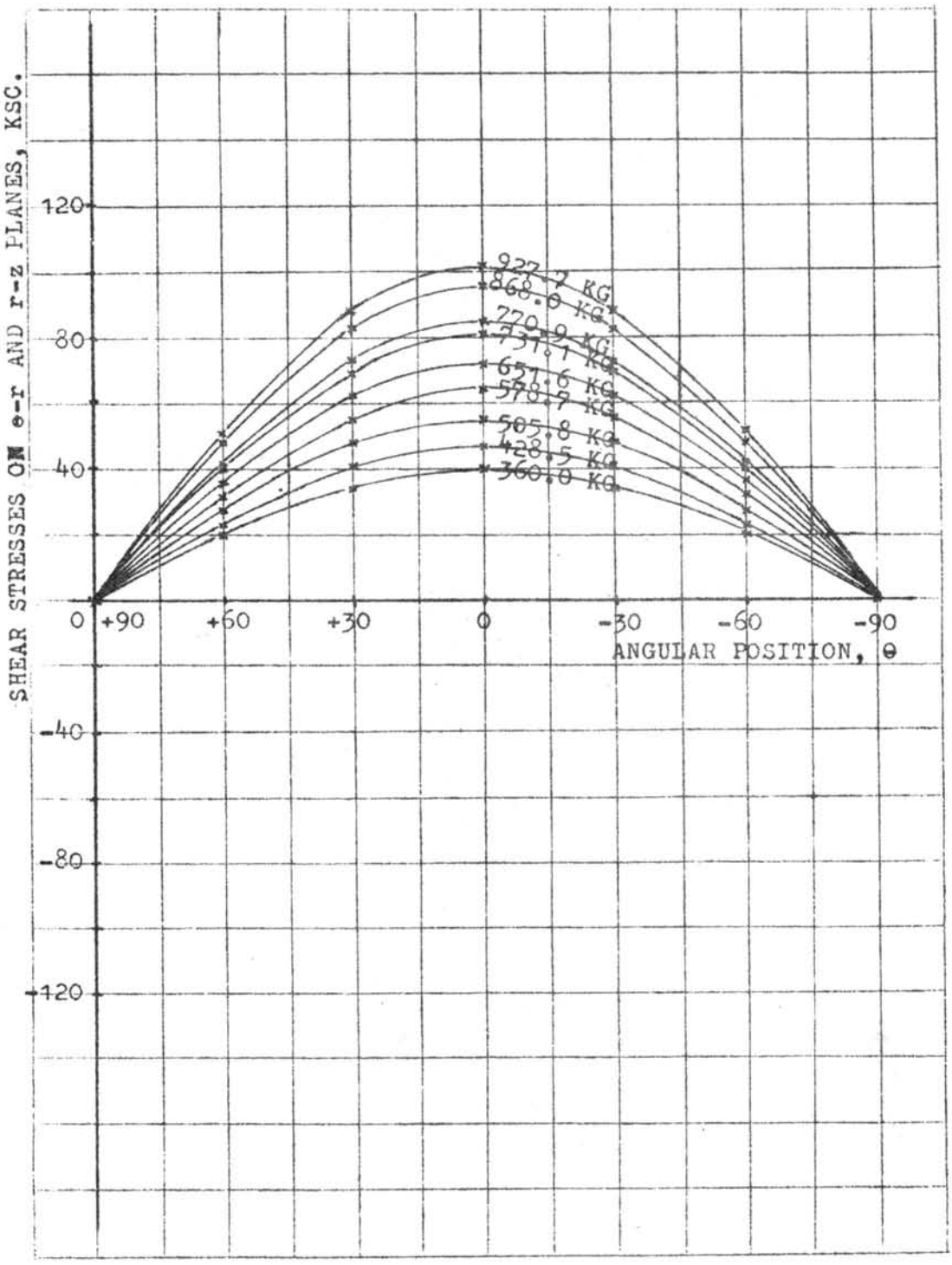

Fig. A18. VARIATION OF SHEAR STRESSES ON θ-r AND r-z PLANES AROUND PIPE.

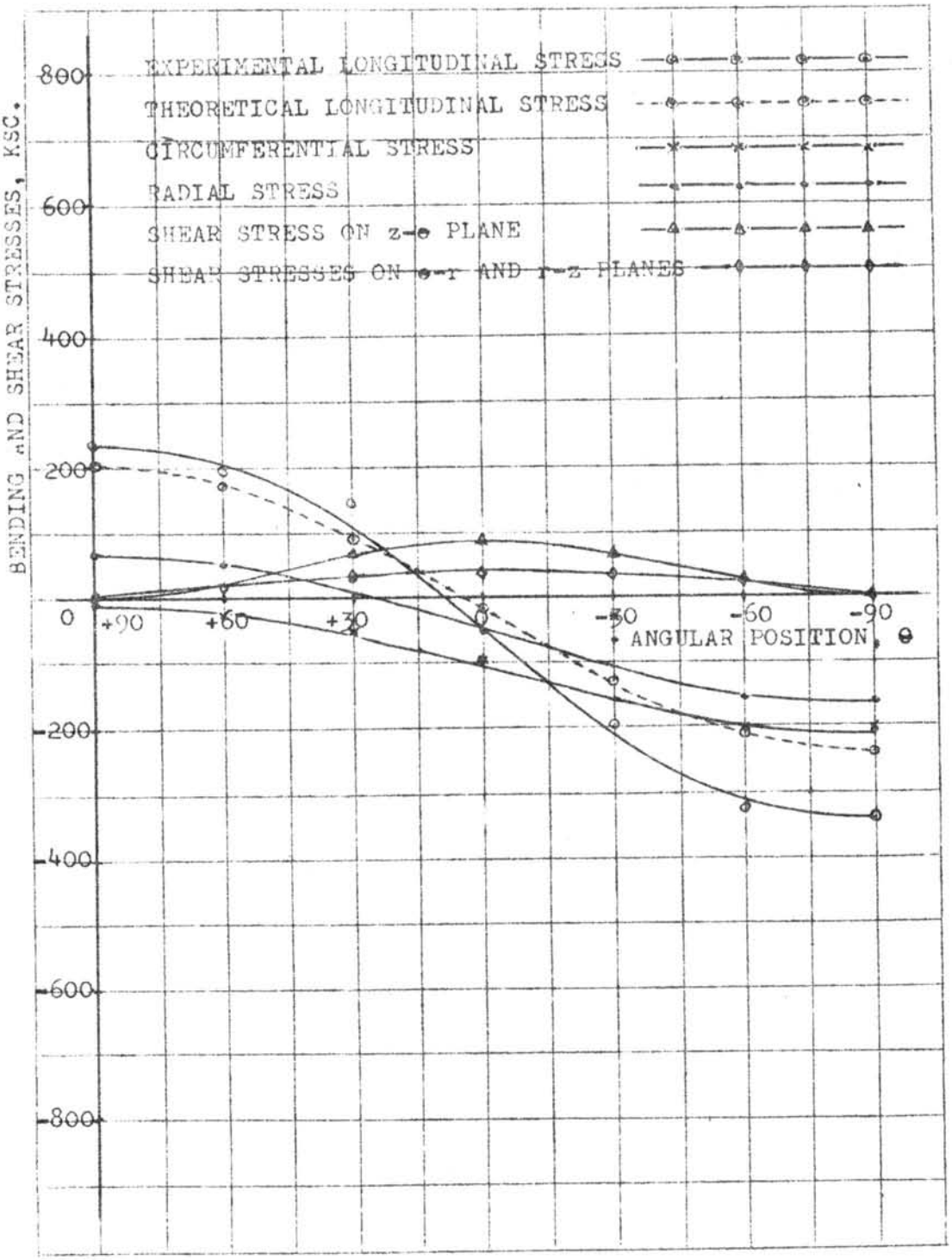

Fig. A19. VARIATION OF BENDING AND SHEAR STRESSES AROUND PIPE.

(AT LOAD 360.0 KG)

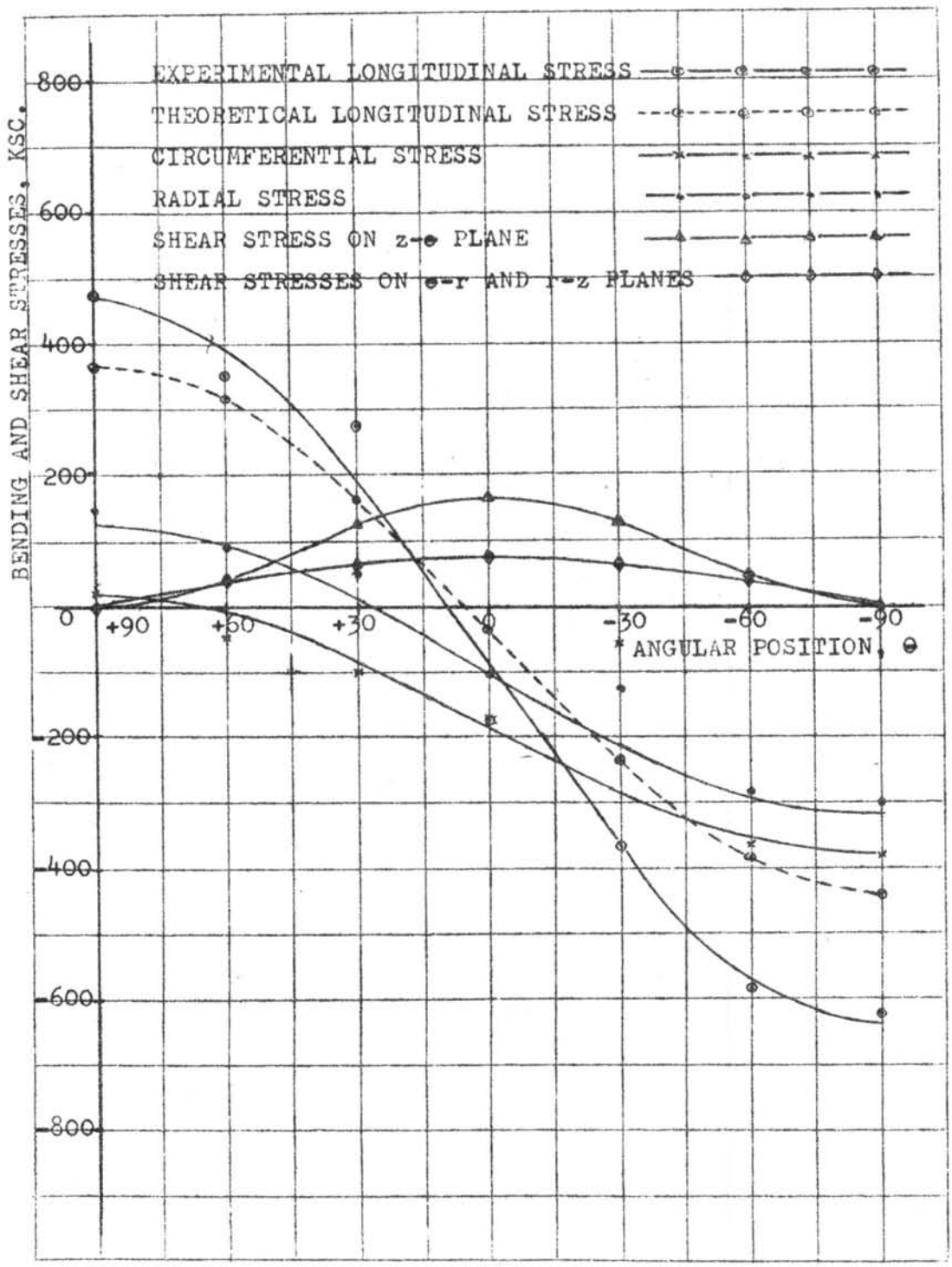

Fig. A20. VARIATION OF BENDING AND SHEAR STRESSES AROUND PIPE.

(AT LOAD 651.6 KG)

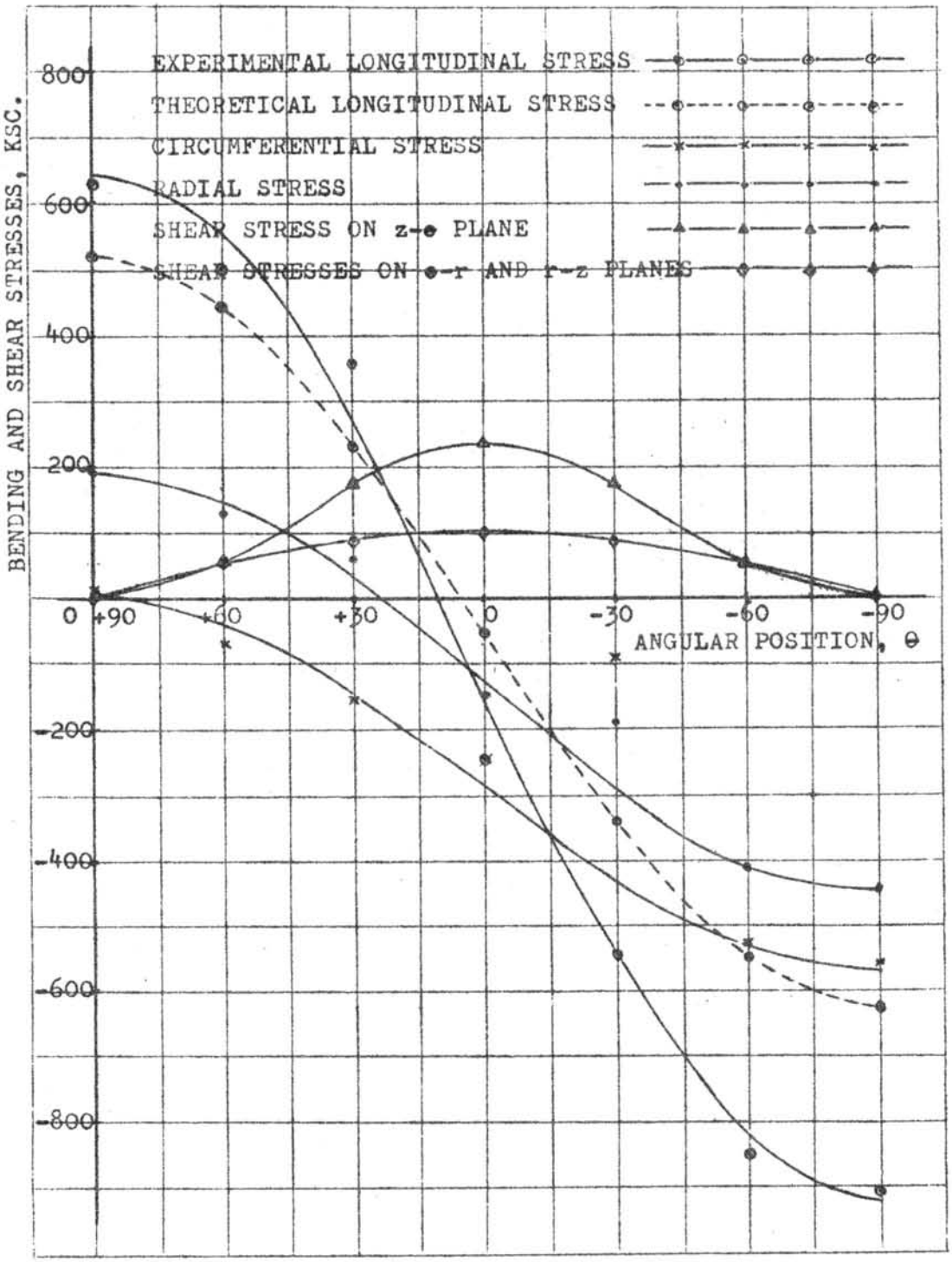

Fig. A21. VARIATION OF BENDING AND SHEAR STRESSES AROUND PIPE.

(AT LOAD 927.7 KG)

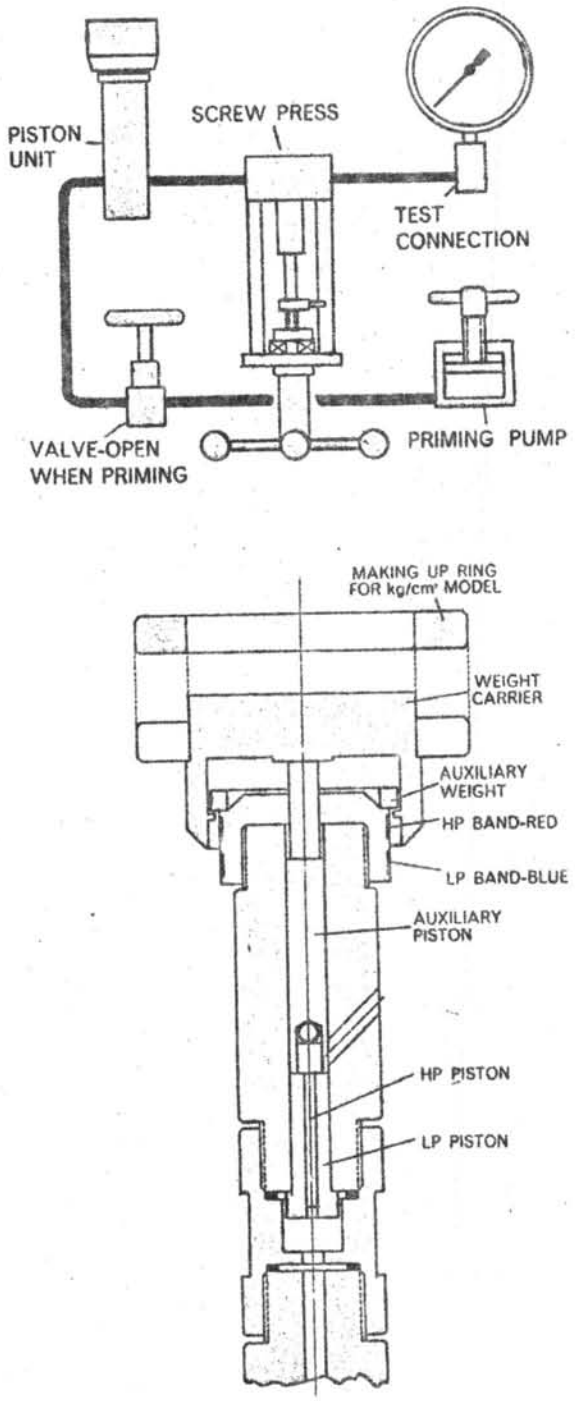

Fig. A22. SECTION DIAGRAM OF BUDENBERG DEAD WEIGHT PRESSURE TESTER.

NOTE:- When used with external Apex Unit open link between terminals 2 and 3

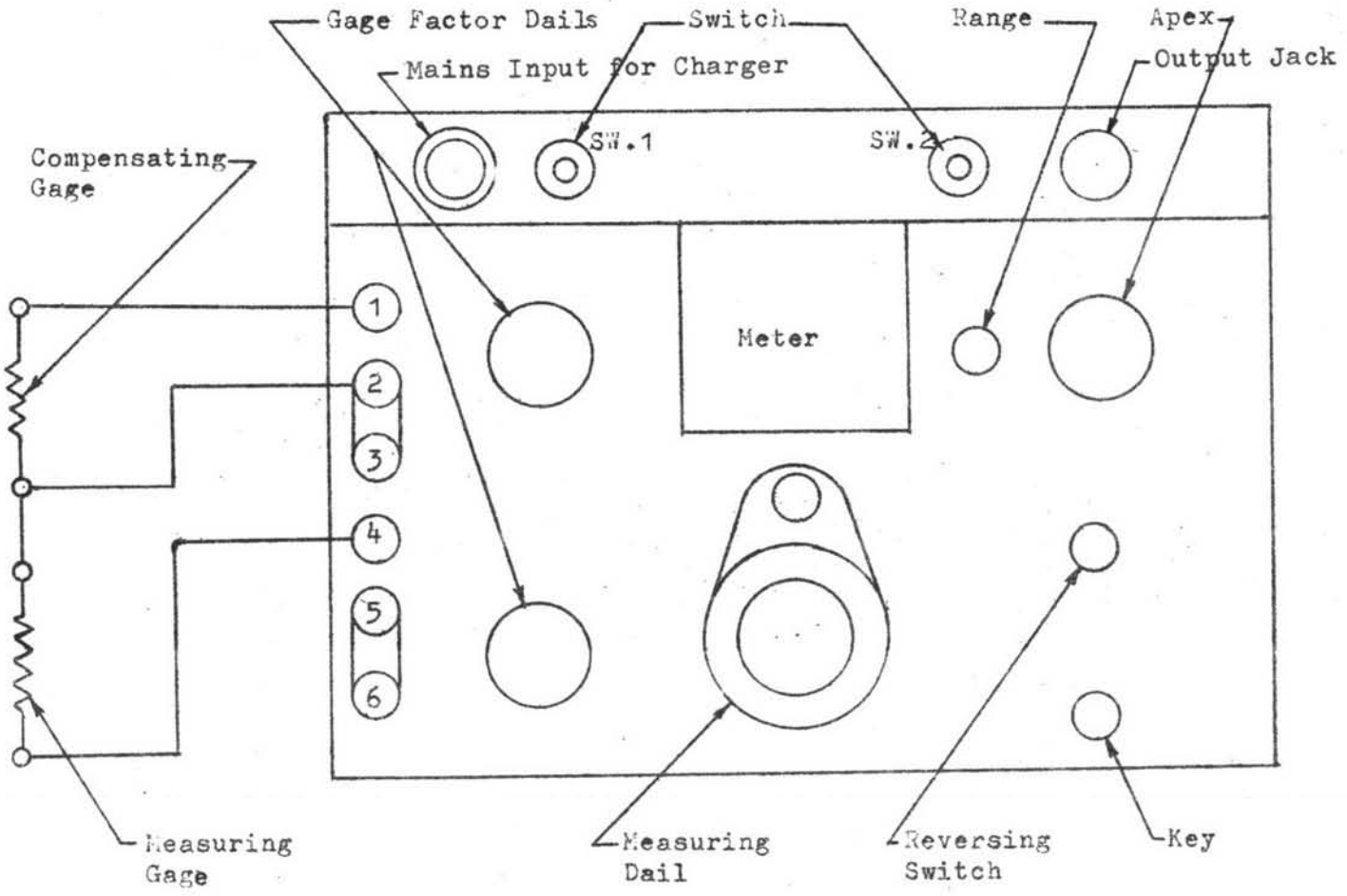

Fig. A23. STRAIN GAGE BRIDGE CONNECTIONS FOR TWO ARM BRIDGE.

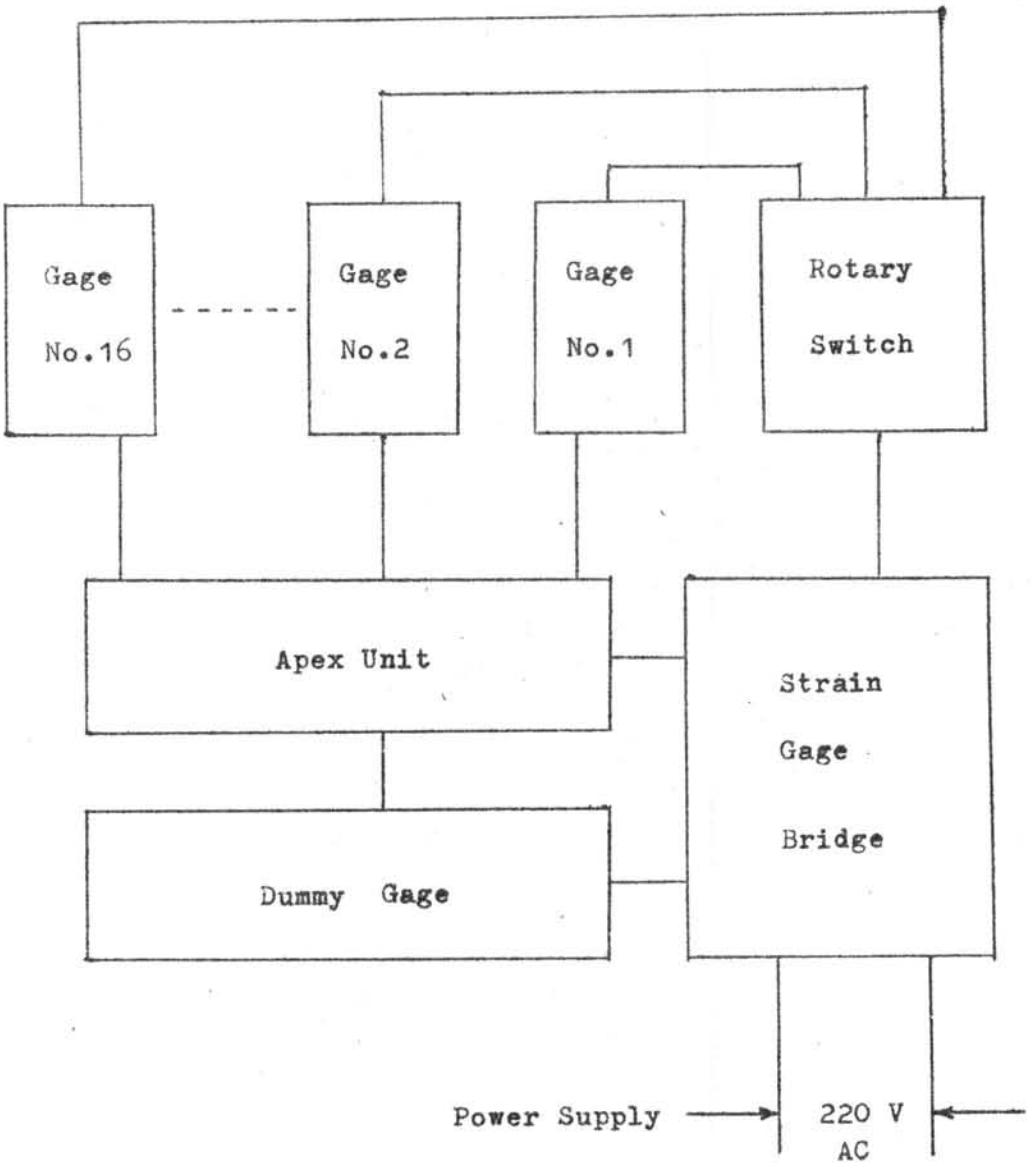

Fig. A24. SCHEMATIC DIAGRAM OF STRAIN MEASUREMENT.

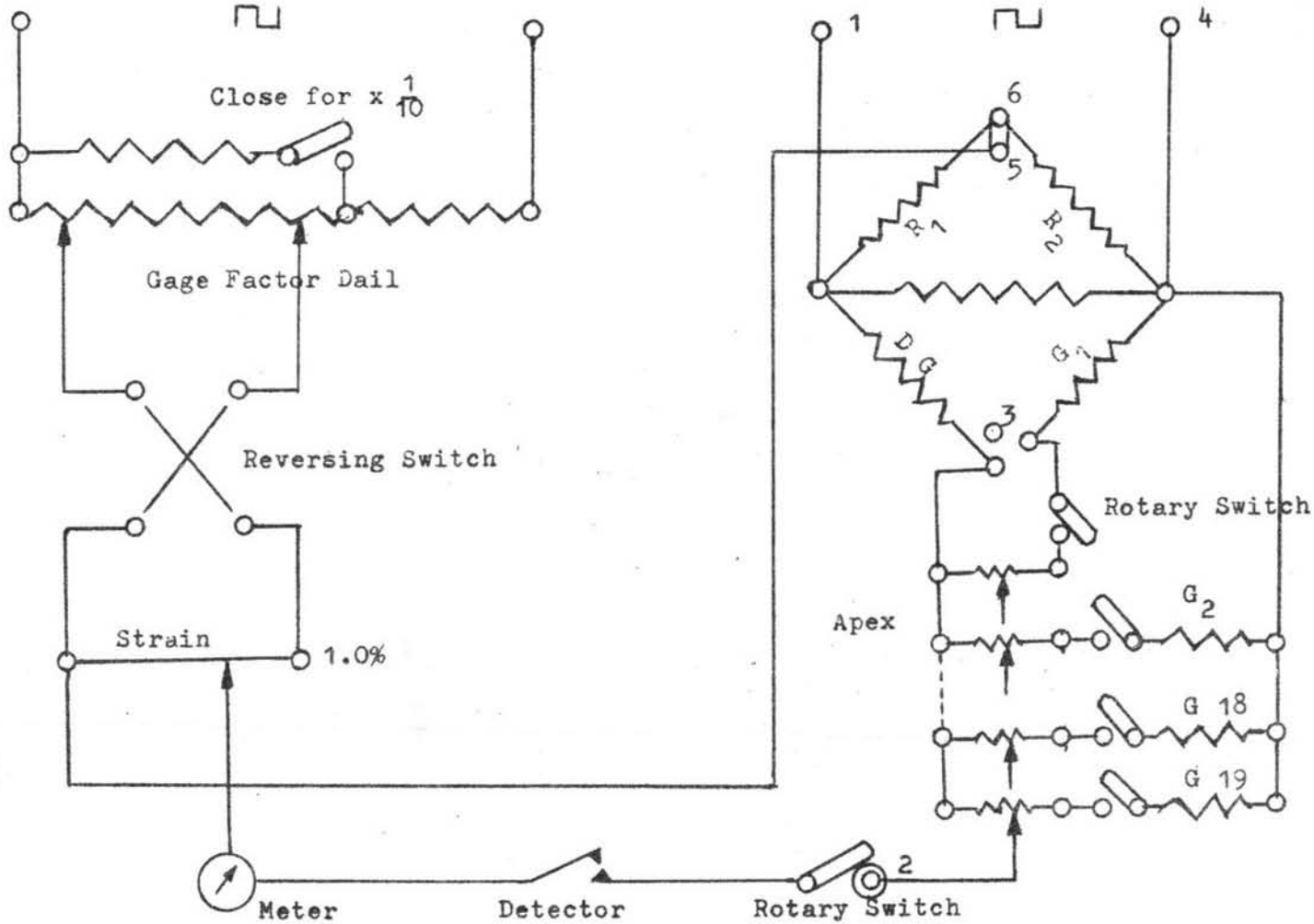

Fig. A25. STRAIN GAGE BRIDGE DIAGRAM.

Fig. A26. PROVING RING NO.56180.

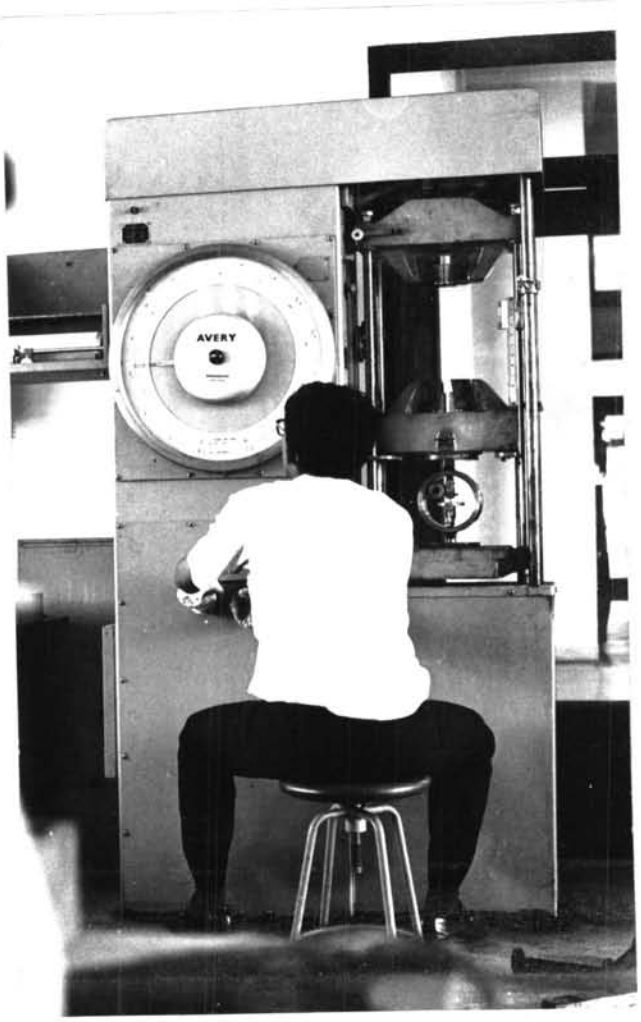

Fig. A27. THE CALIBRATION OF "AVERY" UNIVERSAL TESTING MACHINE BY PROVING RING.

Fig. A28. THE CALIBRATION OF "AMSLER" UNIVERSAL TESTING MACHINE BY PROVING RING.

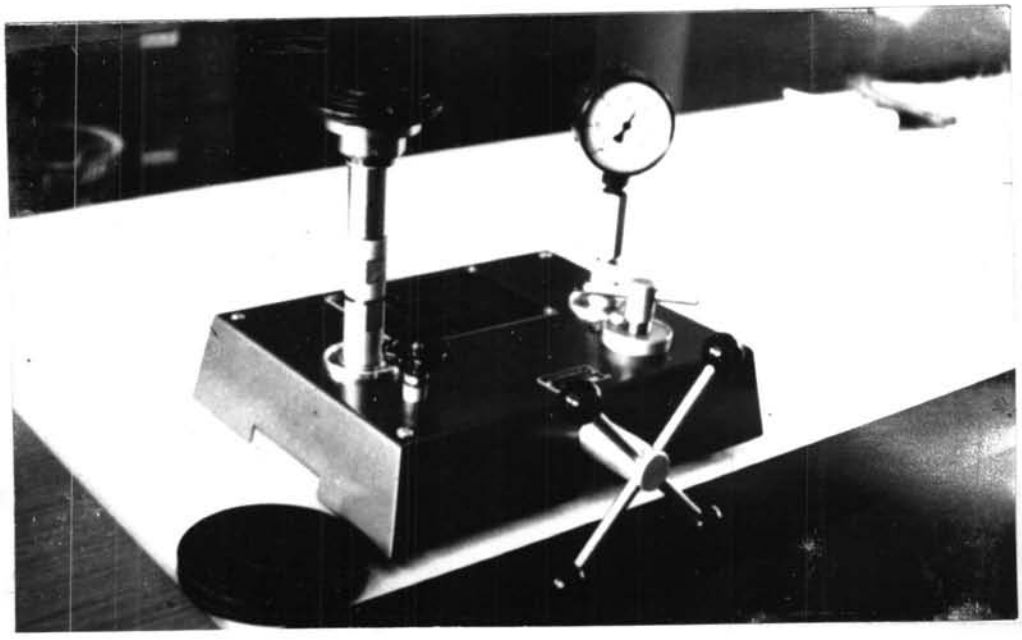

Fig. A29. BUDENBERG PRESSURE GAGE TESTER.

Fig. A30. REINFORCED PIPE BEND.

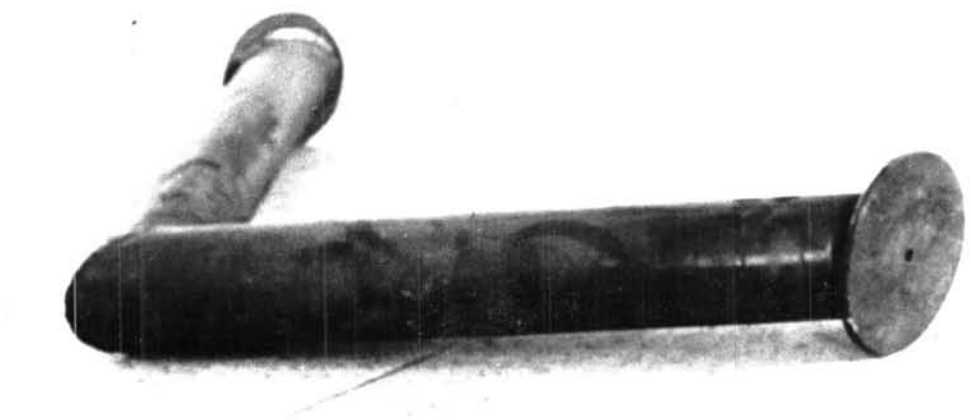

Fig. A31. UNREINFORCED PIPE BEND.

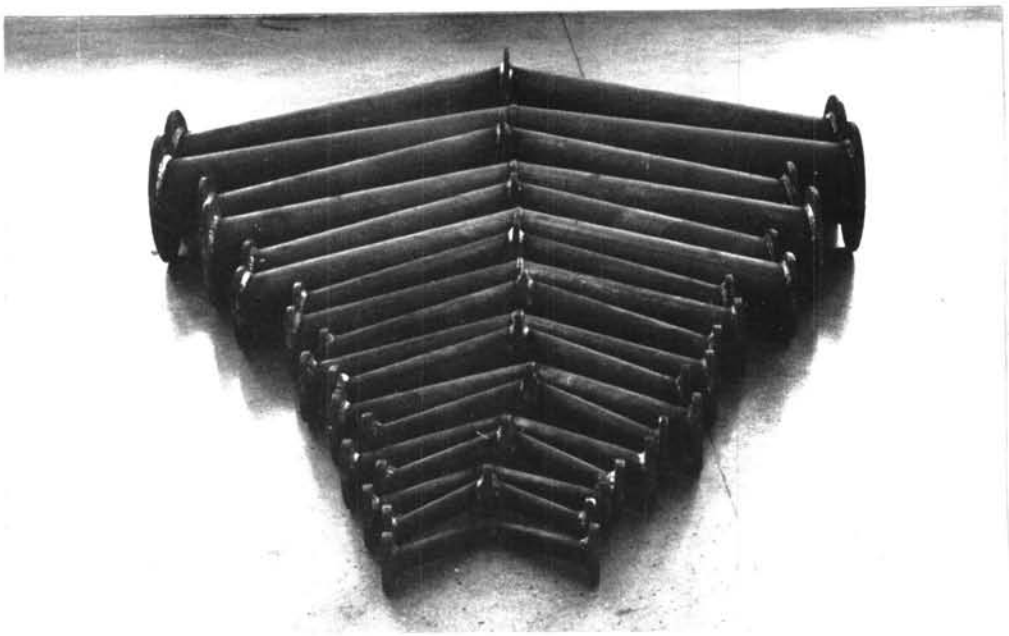

Fig. A32. TEST SPECIMENS.

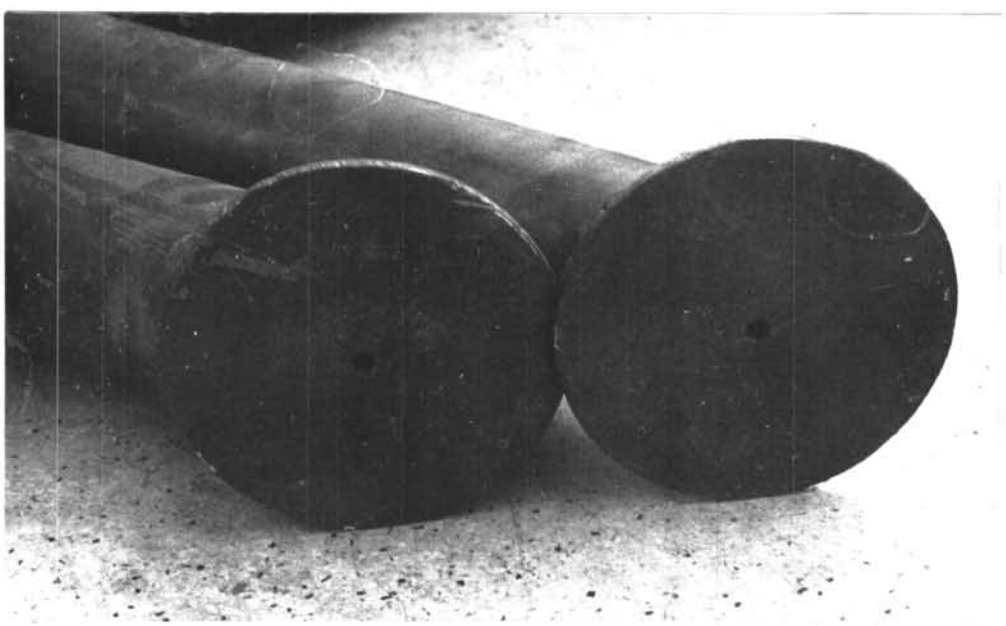

Fig. A33. END VIEW OF THE BENDS.

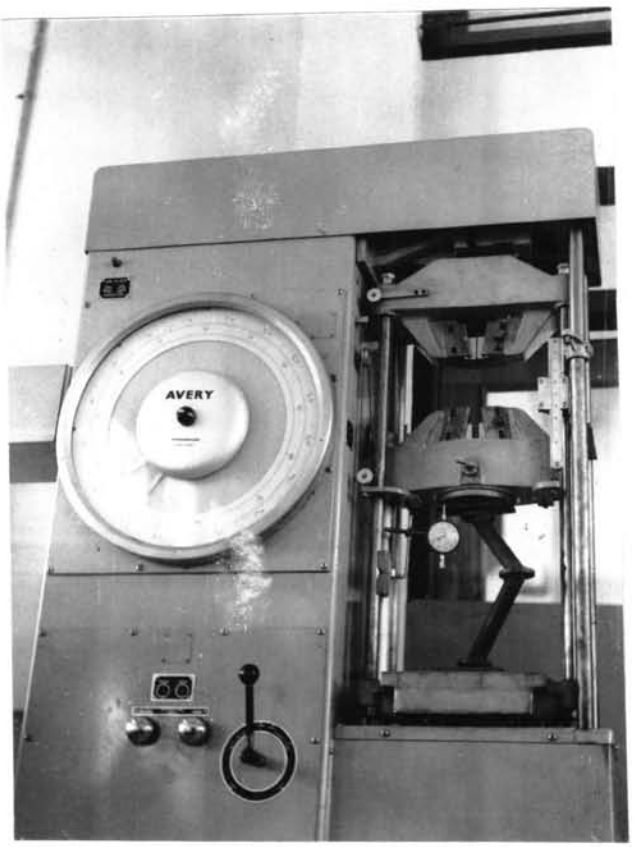

Fig. A34. PIPE BEND UNDER IN-PLANE BENDING LOAD OF AVERY TESTING MACHINE.

Fig. A35. PIPE BEND UNDER IN-PLANE BENDING LOAD OF AMSLER TESTING MACHINE.

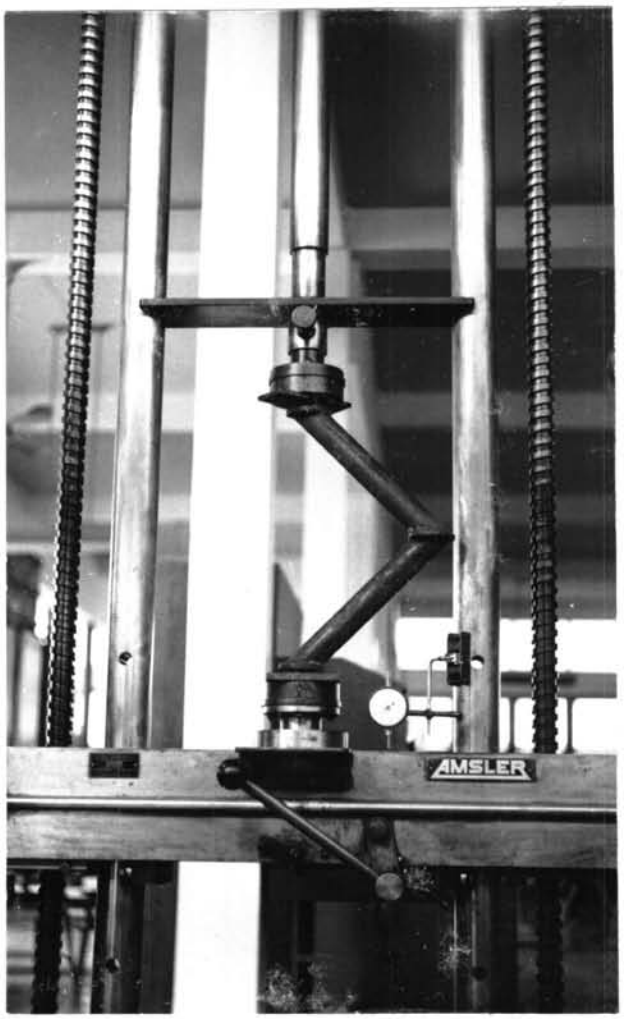

Fig. A36. PIPE BEND UNDER IN-PLANE BENDING LOAD OF AMSLER TESTING MACHINE.

Fig. A37. PIPE BEND UNDER IN-PLANE BENDING LOAD OF SIGURD STENHØJ TESTING MACHINE.

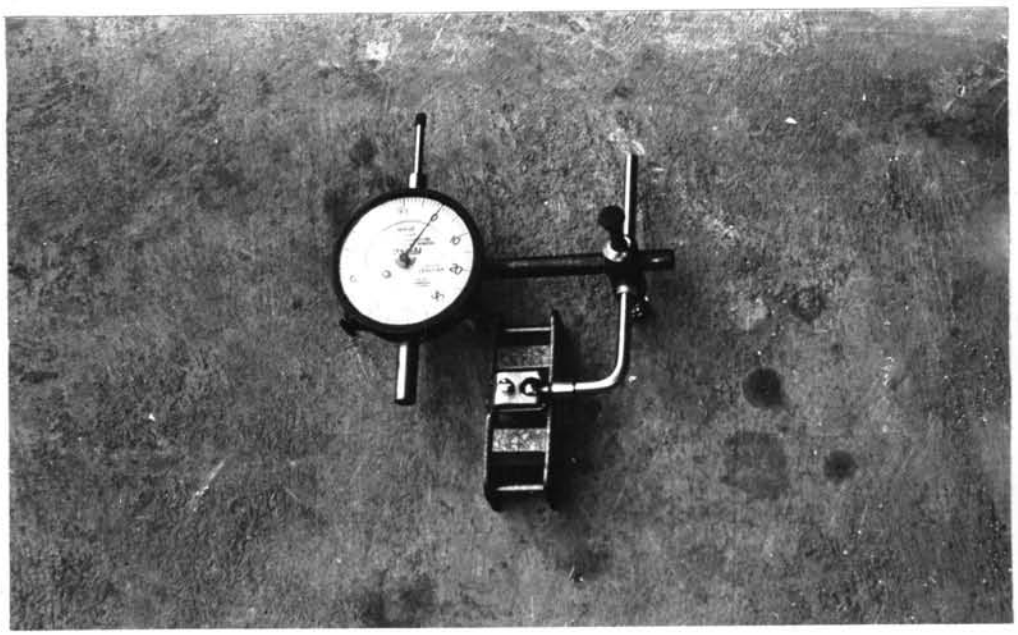

Fig. A38. DIAL GAGE WITH MAGNETIC HOLDER.

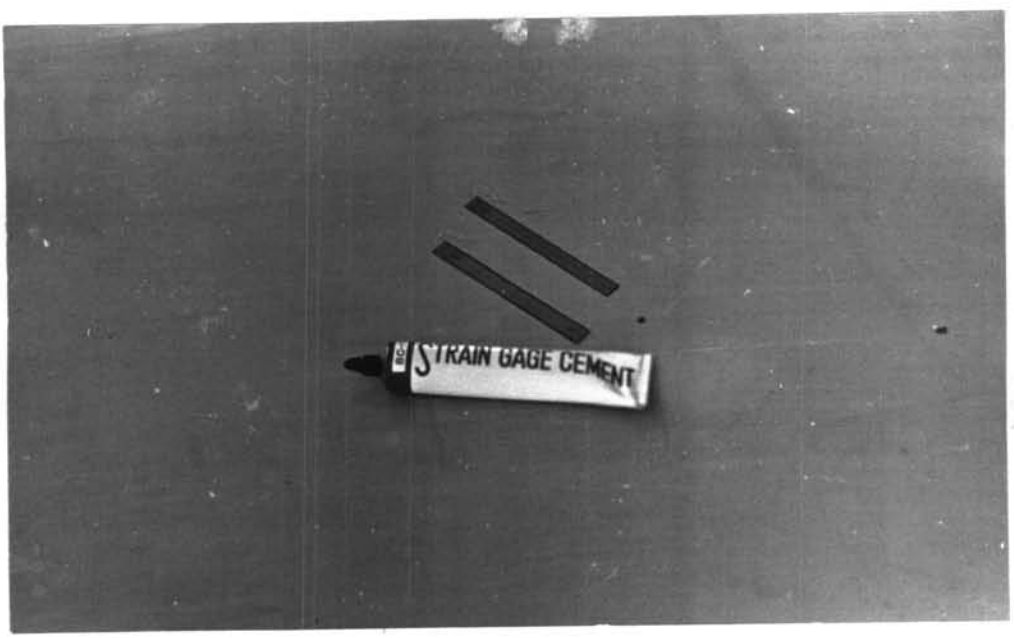

Fig. A39. STRAIN GAGES AND CEMENT.

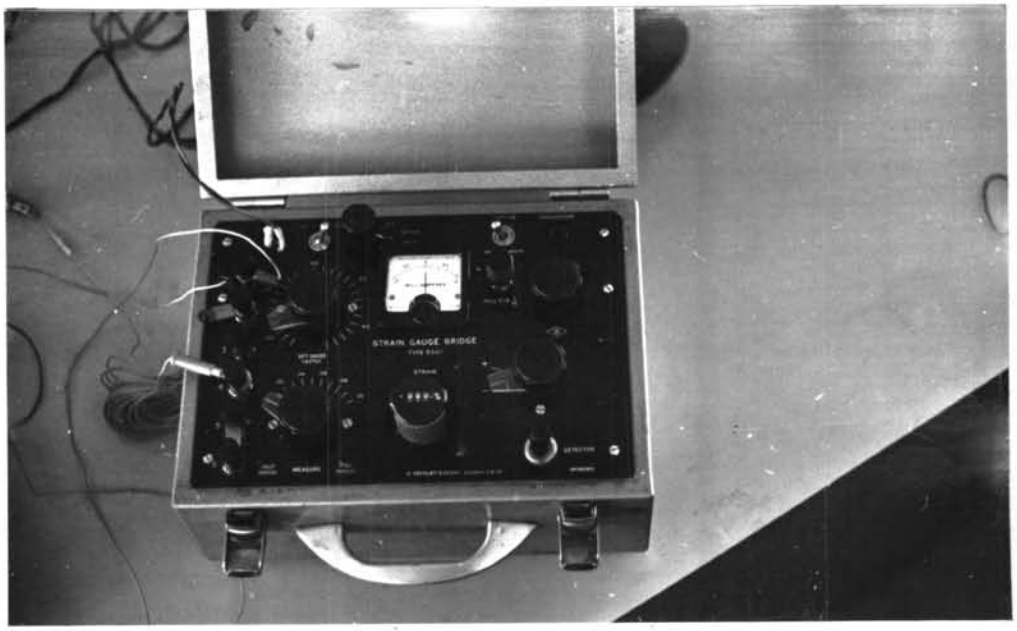

Fig. A40. STRAIN GAGE BRIDGE.

Fig. A41. SELECTOR SWITCH AND APEX UNITS.

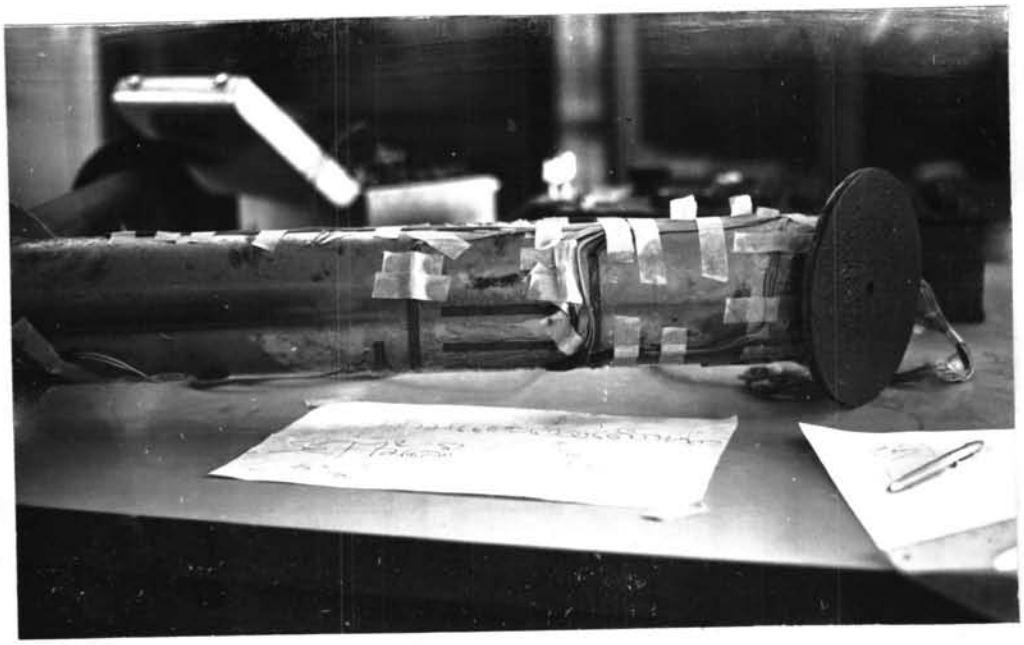

Fig. A42. GAGE POSITIONS FOR THE MEASURING OF LONGITUDINAL AND CIRCUMFERENTIAL STRAINS.

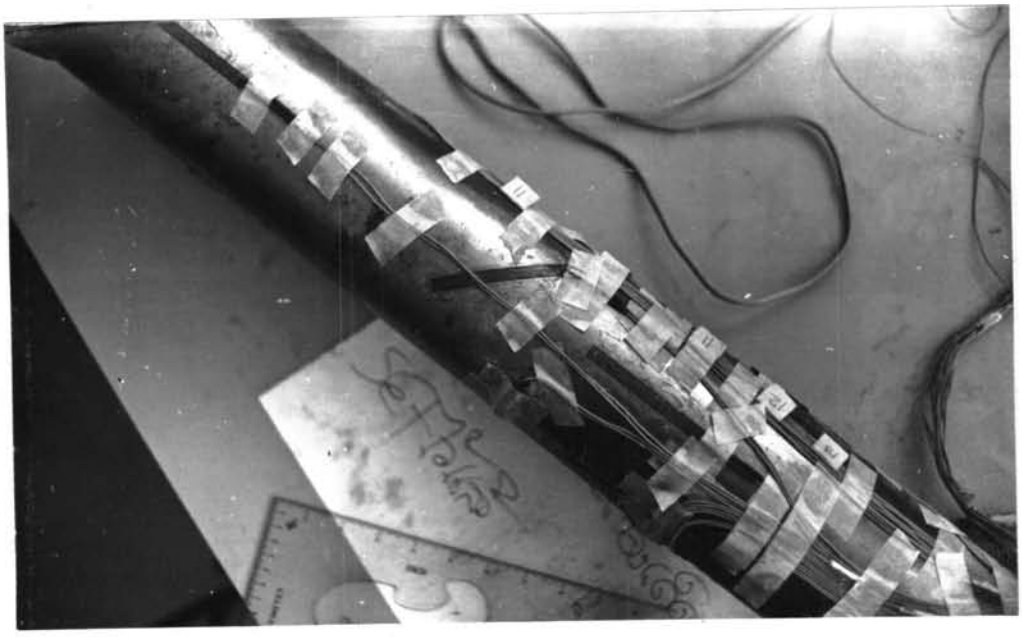

Fig. A43. GAGE POSITION FOR THE MEASURING OF PRINCIPAL STRAIN AT ZERO DEGREE POSITION.

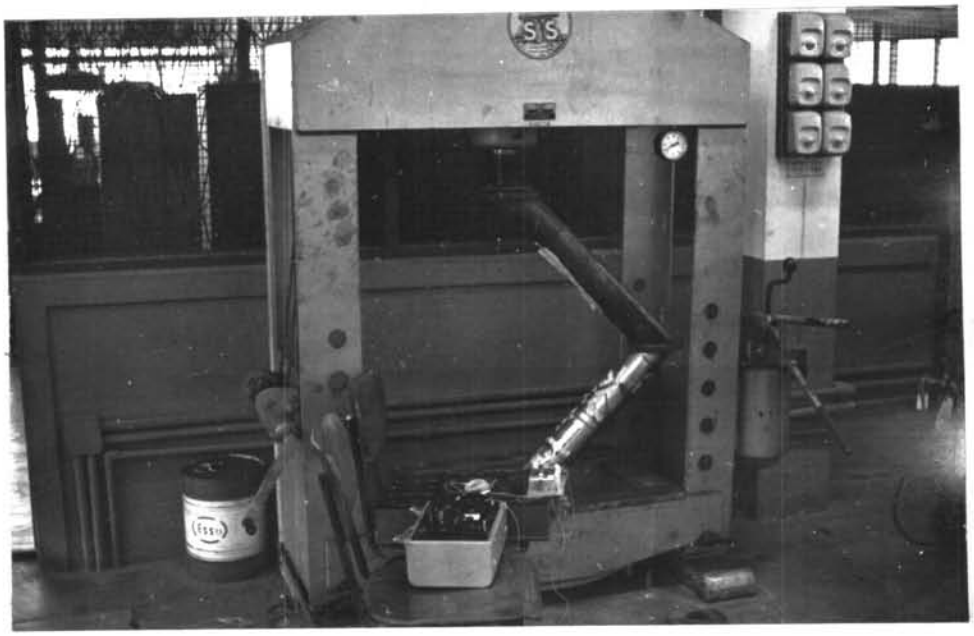

Fig. A44. THE MEASUREMENT OF STRAINS BY STRAIN-GAGE TECNIQUE.